

MESOSCALE CONVECTIVE COMPLEXES (MCC): SATELLITE-BASED OBSERVATIONS

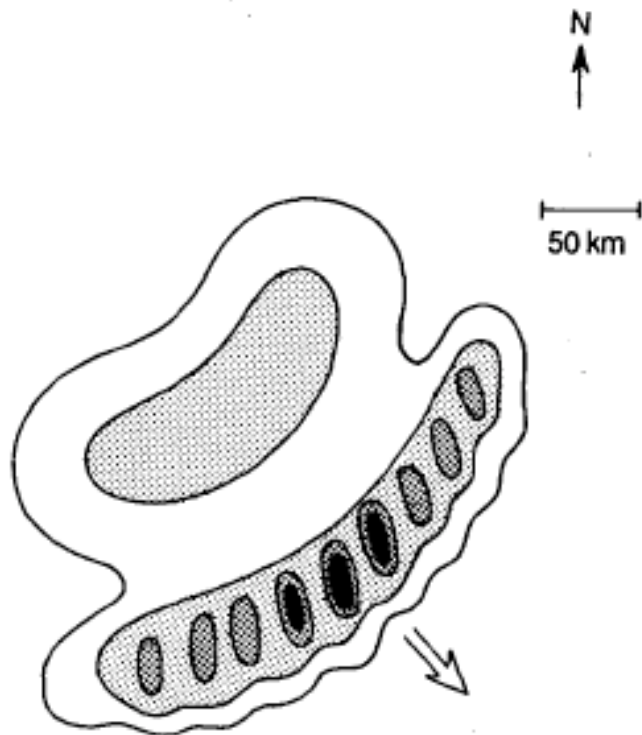
- AREA OF COLD IR TOPS, SHAPE,  $\geq 6$  hrs  
(Maddox 1980)

MESOSCALE CONVECTIVE SYSTEMS (MCS): RADAR-BASED OBSERVATIONS

MOIST CONVECTIVE OVERTURNING, MESOSCALE  
CIRCULATION, AT LEAST PARTIALLY DRIVEN BY  
CONVECTIVE PROCESSES (Zipser 1982)

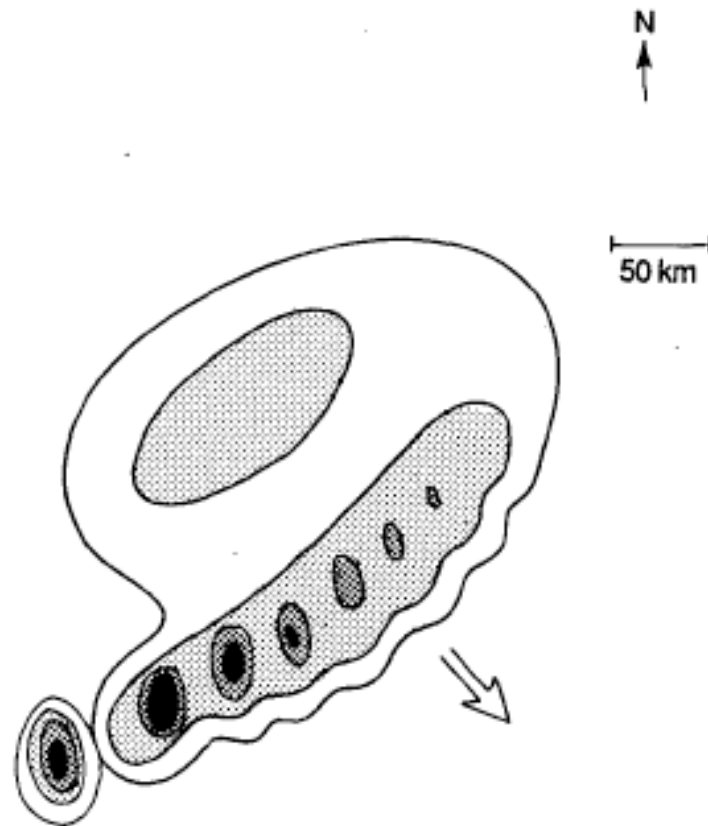
QUASI-LINEAR MESOSCALE CONVECTIVE SYSTEMS (SQUALL LINES)

## STRUCTURE



### SYMMETRIC CASE

FIG. 7. Schematic depicting Symmetric type of leading-line/trailing-stratiform mesoscale precipitation system organization. Large vector indicates direction of system motion. Levels of shading denote increasing radar reflectivity, with most intense values corresponding to convective cell cores. Horizontal scale and north arrow are shown.



### ASYMMETRIC CASE

FIG. 8. As in Fig. 7 except for Asymmetric type of leading-line/trailing-stratiform mesoscale precipitation system organization.

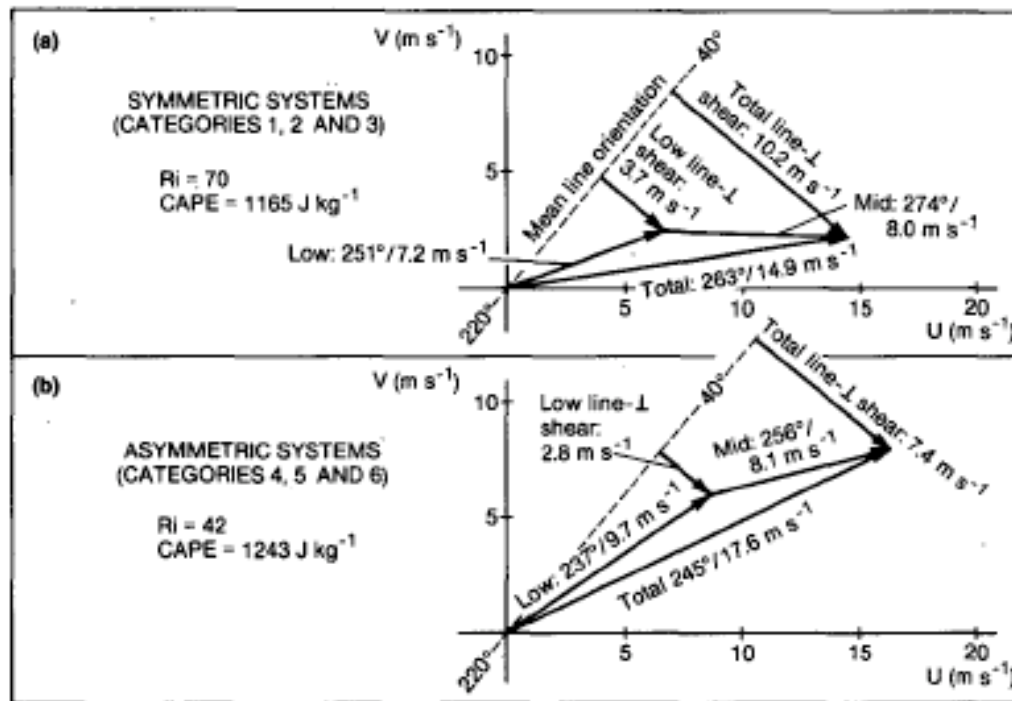


FIG. 25. As in Fig. 24, except for (a) Symmetric systems (Categories 1, 2 and 3), and (b) Asymmetric systems (Categories 4, 5 and 6).

**CLASSIFICATION OF SQUALL-LINE DEVELOPMENT**





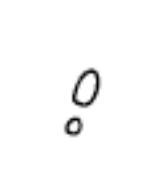


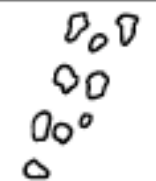




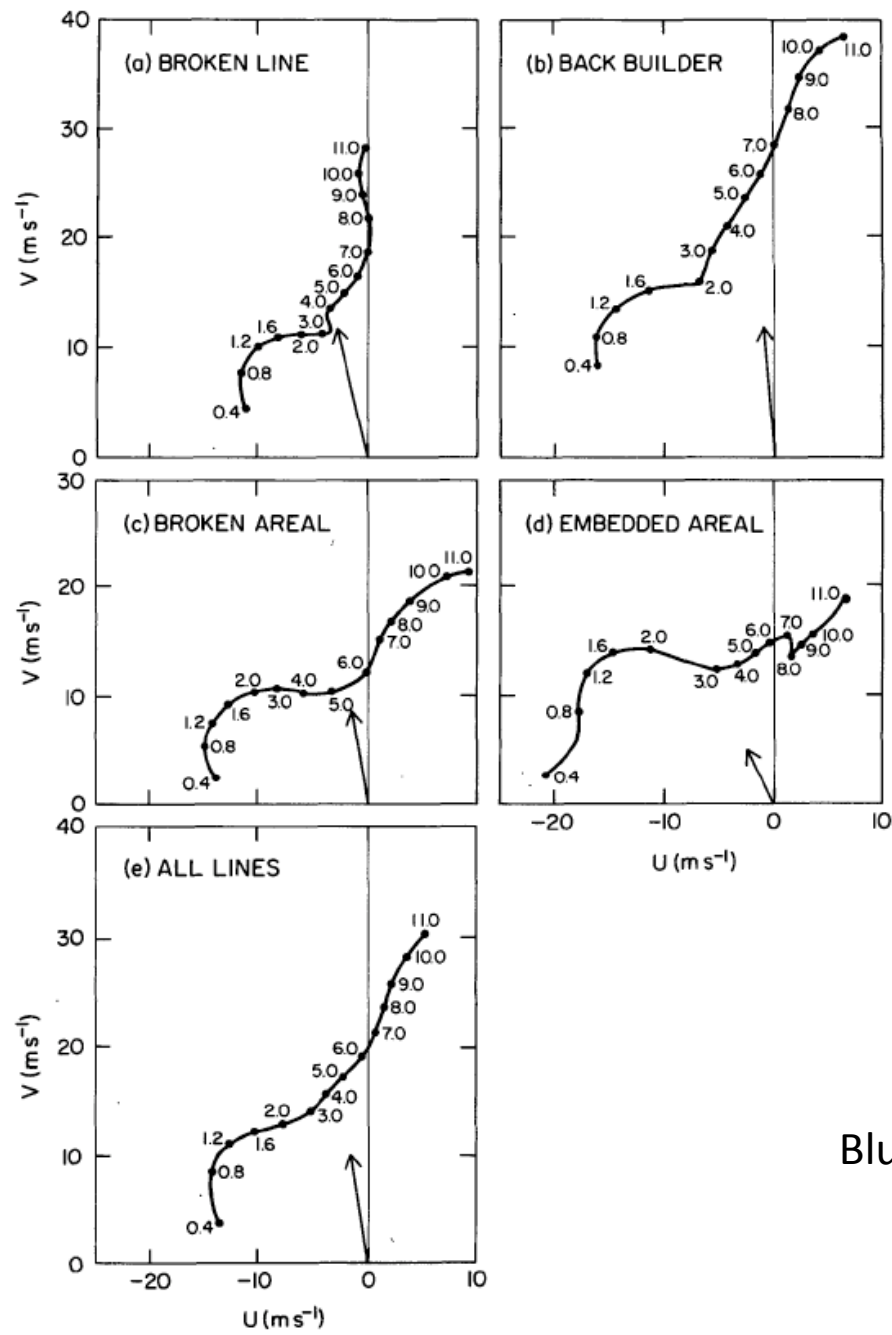
<p><b>BROKEN LINE</b> (14 Cases)</p>			
<p><b>BACK BUILDING</b> (13 Cases)</p>			
<p><b>BROKEN AREAL</b> (8 Cases)</p>			
<p><b>EMBEDDED AREAL</b> (5 Cases)</p>			
	$t=0$	$t=\Delta t$	$t=2\Delta t$

FIG. 1. Idealized depiction of squall-line formation.

Bluestein and Jain 1985



Bluestein and Jain 1985

FIG. 14. Composite hodographs in coordinate system moving along with the line (squall-line coordinates).

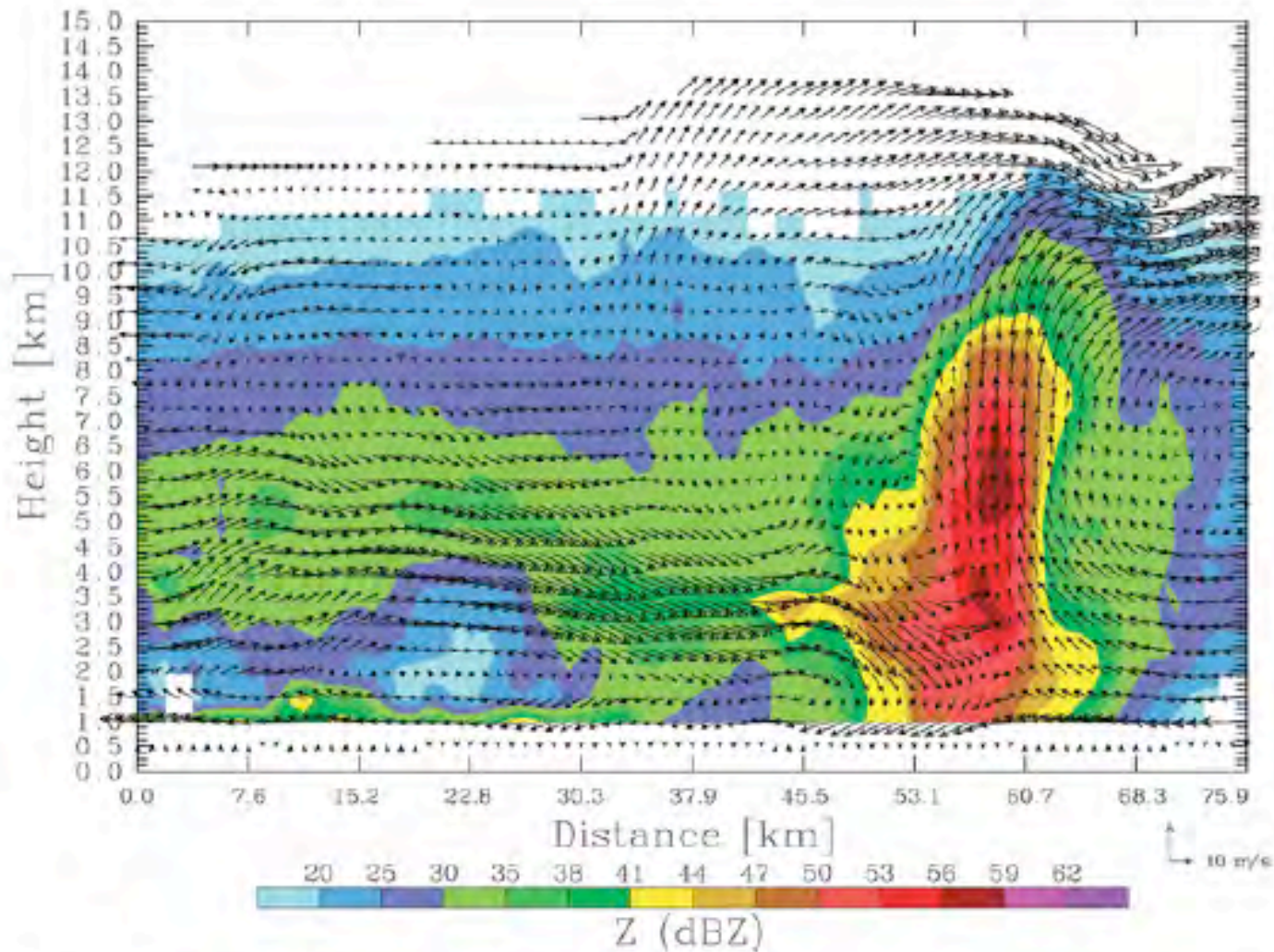


**FIG. 6.** Cross section from 10 Jun bow echo (see Fig. 5b) produced from quad-Doppler analysis. Shown are system-relative winds and reflectivity (dBZ) in the vertical plane.

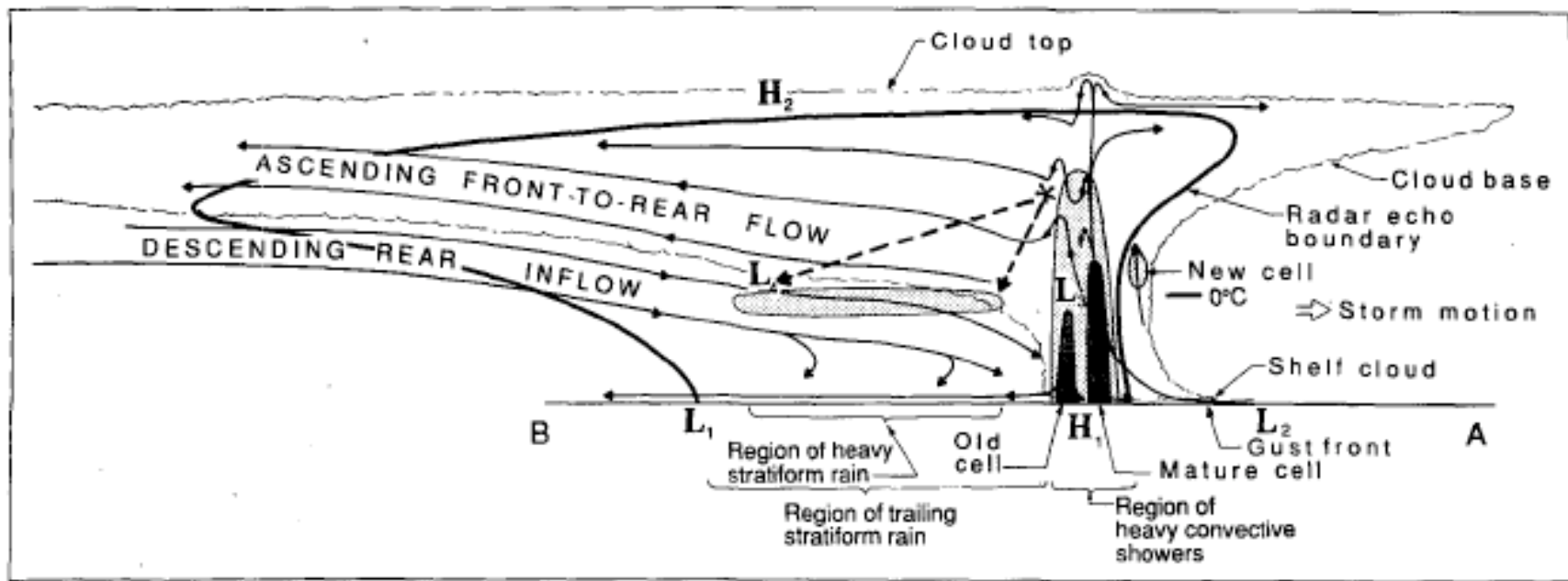


FIG. 1. Conceptual model of a squall line with a trailing stratiform area viewed in a vertical cross section oriented perpendicular to the convective line (i.e., parallel to its motion). See text for further explanation.

Houze et al. 1989



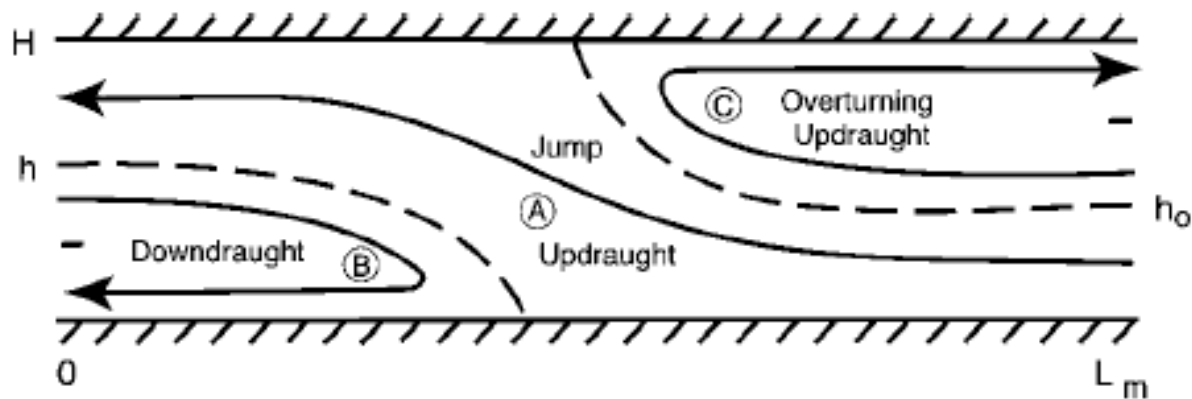


FIG. 3. Theoretical two-dimensional model of a convective line depicting both jump and overturning updrafts, redrafted from Moncrieff (1992).

Parker and Johnson 2000

See example in Emanuel's text



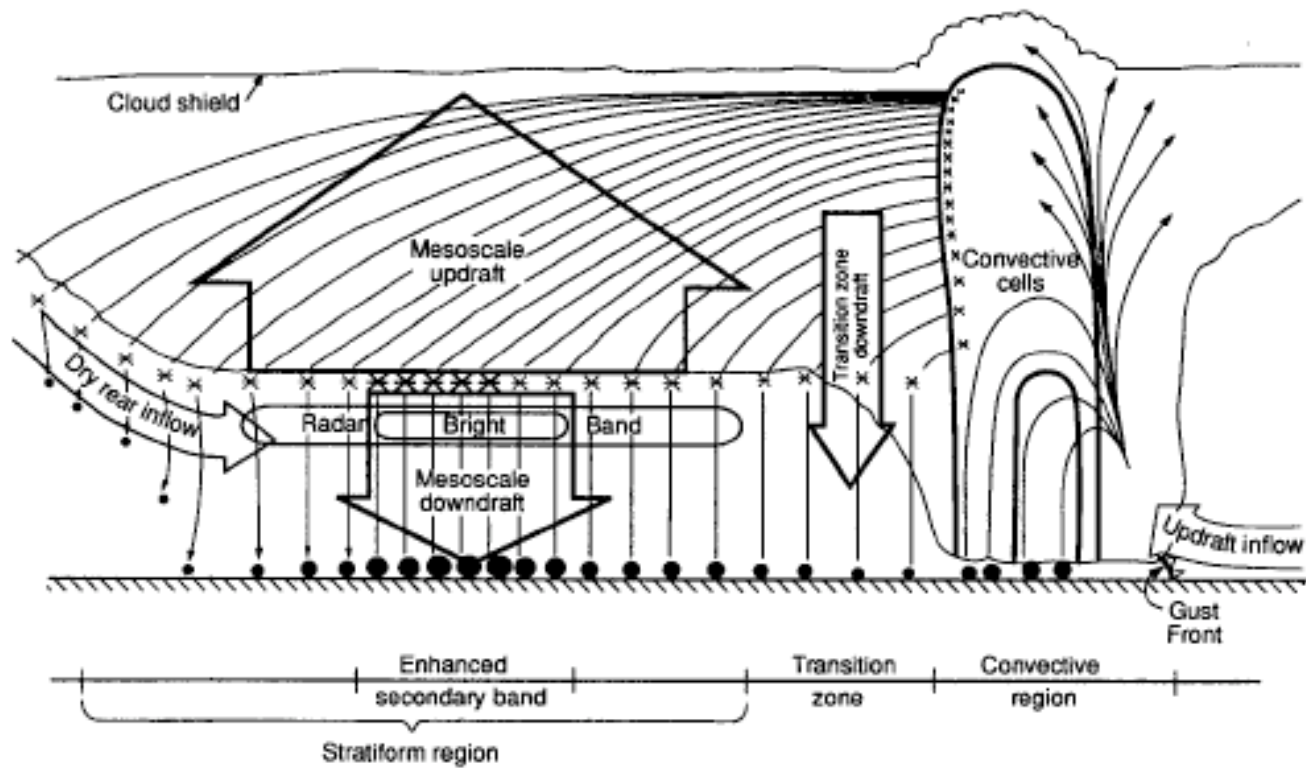


FIG. 1. Conceptual model of precipitation particle trajectories and mean vertical motions through the trailing stratiform region of a squall-line system.

Biggerstaff and Houze 1991

HYPOTHESES FOR TRANSITION-ZONE REFLECTIVITY MINIMUM AND SECONDARY, STRATIFORM MAXIMUM: *FOR DETAILS, SEE BRAUN AND HOUZE (1994)*

1. DOWNWARD MOTION IN TRANSITION ZONE: **SUPPRESSED GROWTH IN DESCENT AREA**
  - EVAPORATION DUE TO DOWNDRAFT
  - ENHANCED DESCENT
  - LACK OF GROWTH, VAPOR DEPOSITION INHIBITED, SMALL ICE PARTICLES ABSENT
  
2. TRAJECTORIES OF ICE PARTICLES DETAINED FROM UPPER LEVELS OF CONVECTIVE CELLS IN LEADING LINE; KINEMATIC CONSEQUENCE OF WHERE PRECIP. PARTICLES FROM CELLS IN LEADING LINE FALL OUT AS A RESULT OF THEIR TERMINAL FALL SPEEDS AND HORIZONTAL WIND: **FALLOUT PATTERN OF PRECIP. PARTICLES DETAINED FROM CONVECTIVE CELLS**
  - DIFFERENTIAL FALL SPEEDS FOR SNOW, GRAUPEL
  - VERTICAL DISTRIBUTION OF ICE DETAINED FROM LEADING LINE CELLS
  
3. MESOSCALE UPWARD MOTION: **ENHANCED GROWTH OF PRECIP. PARTICLES WITHIN MESOSCALE UPDRAFT** (MOST IMPORTANT)
  - LONGER RESIDENCE TIME IN UPPER-LEVEL, MESOSCALE UPDRAFT, ABOVE MELTING LEVEL
  - PASSAGE OF PARTICLES THROUGH REGION OF ENHANCED ASCENT AT LEADING EDGE OF SECONDARY BAND
  - TRAJECTORIES OF ICE PARTICLES FROM LEADING LINE THROUGH MESOSCALE UPDRAFT

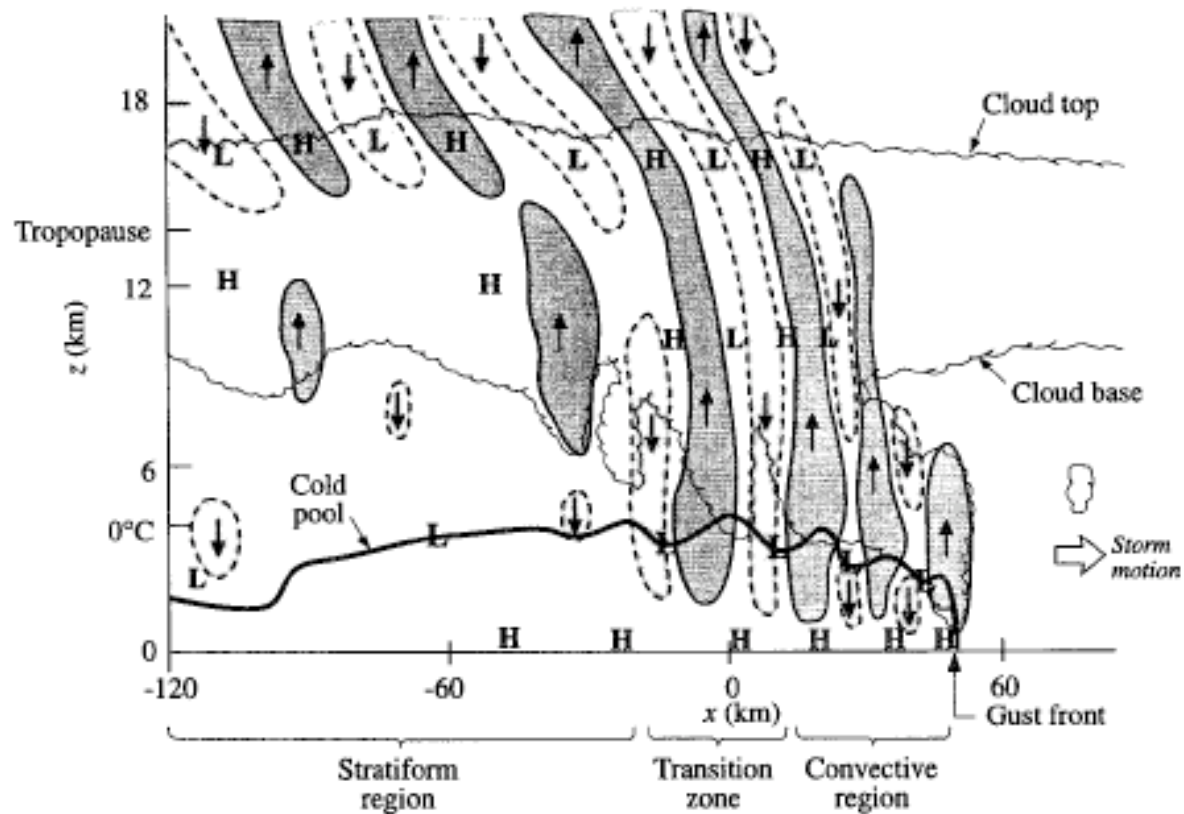


FIG. 25. Schematic model of the gravity wave structure for a mature-stage multicellular squall line based on 2D simulation results at  $t = 11$  h. Updrafts greater than  $1 \text{ m s}^{-1}$  are heavily shaded, and downdrafts less than  $-1 \text{ m s}^{-1}$  are lightly shaded. Heavy line is the cold pool outline defined by the  $\theta' = -1 \text{ K}$  contour; cloud shield is defined by the  $0.5 \text{ g kg}^{-1}$  contour of nonprecipitating hydrometeor mixing ratio ( $q_c + q_i = 0.5 \text{ g kg}^{-1}$ ;  $q_c$  is the cloud water mixing ratio and  $q_i$  is the cloud ice mixing ratio). A letter L or H denotes a region of low or high pressure.

Yang and Houze 1995 VERTICALLY TRAPPED GRAVITY WAVES

ALTERNATIVE TO FOVELL AND OGURA (1988) HYPOTHESIS

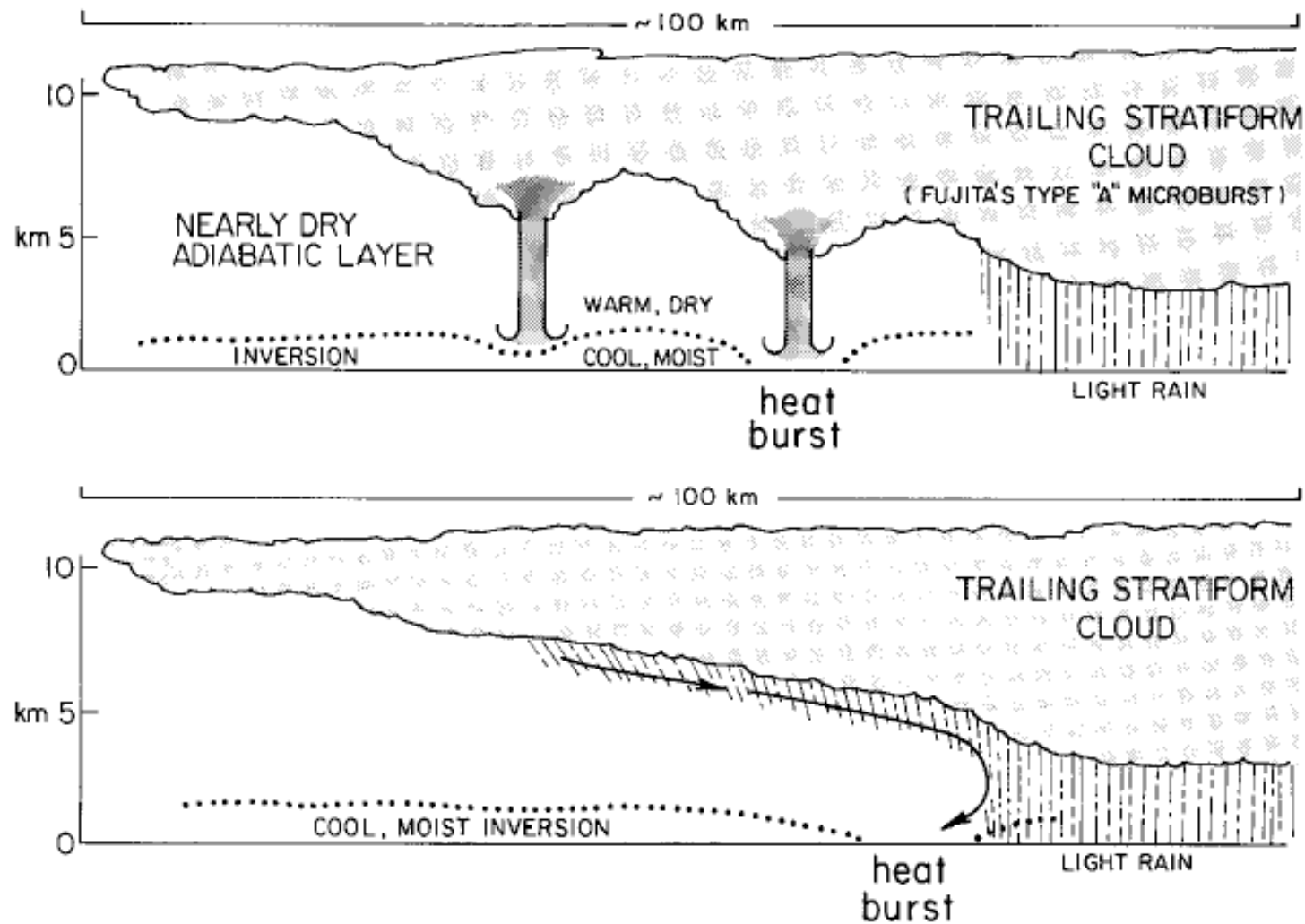
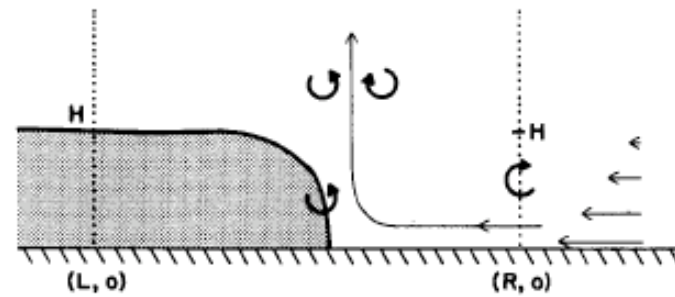
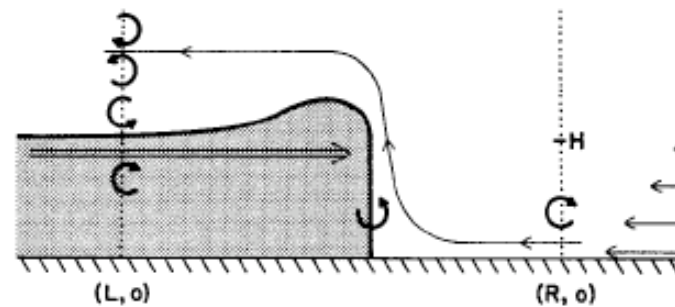


FIG. 19. Depictions of two possible heat burst mechanisms associated with the trailing stratiform regions of mesoscale convective systems: (top) microbursts penetrating shallow surface inversion and (bottom) descending rear- or lateral-inflow jet penetrating surface inversion. Heat bursts can also occur in association with downdrafts from isolated thunderstorms penetrating a surface inversion (not shown).

a) Cold Pool Balanced by Shear



b) Cold Pool with Shear and Elevated Jet



c) Cold Pool with Shear and Surface Jet

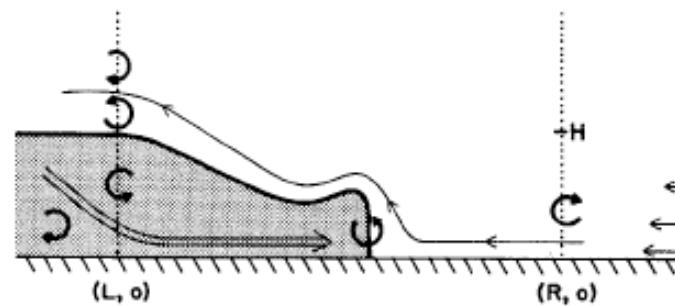


FIG. 15. Schematic depiction of (a) a cold pool spreading in an environment having sufficient vertical wind shear to balance the cold-pool-generated circulation, (b) a cold pool balanced by the ambient vertical wind shear and an elevated rear inflow jet, and (c) a cold pool in the presence of a surface rear-inflow jet. The shading denotes the region of negatively buoyant air. The thick arrows depict the sense of the vorticity that is generated at the leading edge of the cold pool or that is advected through the boundaries.

Weisman 1992

LONGEVITY OF A  
MULTICELL SQUALL  
LINE

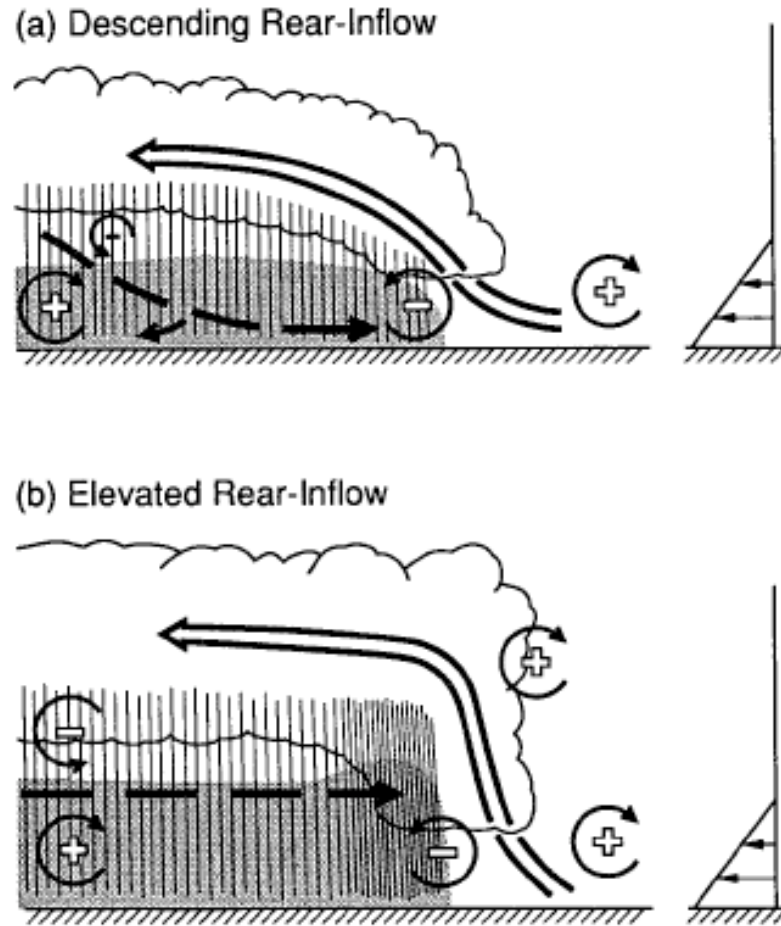


FIG. 23. A conceptual model of the mature structure of a long-lived squall-line-type convective system for (a) a system with a descending rear-inflow jet and (b) a system with an elevated rear-inflow jet. The updraft current is denoted by the thick, double-lined flow vector, while the rear-inflow current is denoted by the thick, dashed flow vector. The shading denotes the surface cold pool. The thin, circular arrows depict the most significant sources of horizontal vorticity, which are either associated with the ambient shear or which are generated within the convective system, as described in the text. Regions of lighter or heavier rainfall are indicated by the more sparsely or densely packed vertical lines, respectively. The scalloped line denotes the outline of the cloud.

Weisman 1992

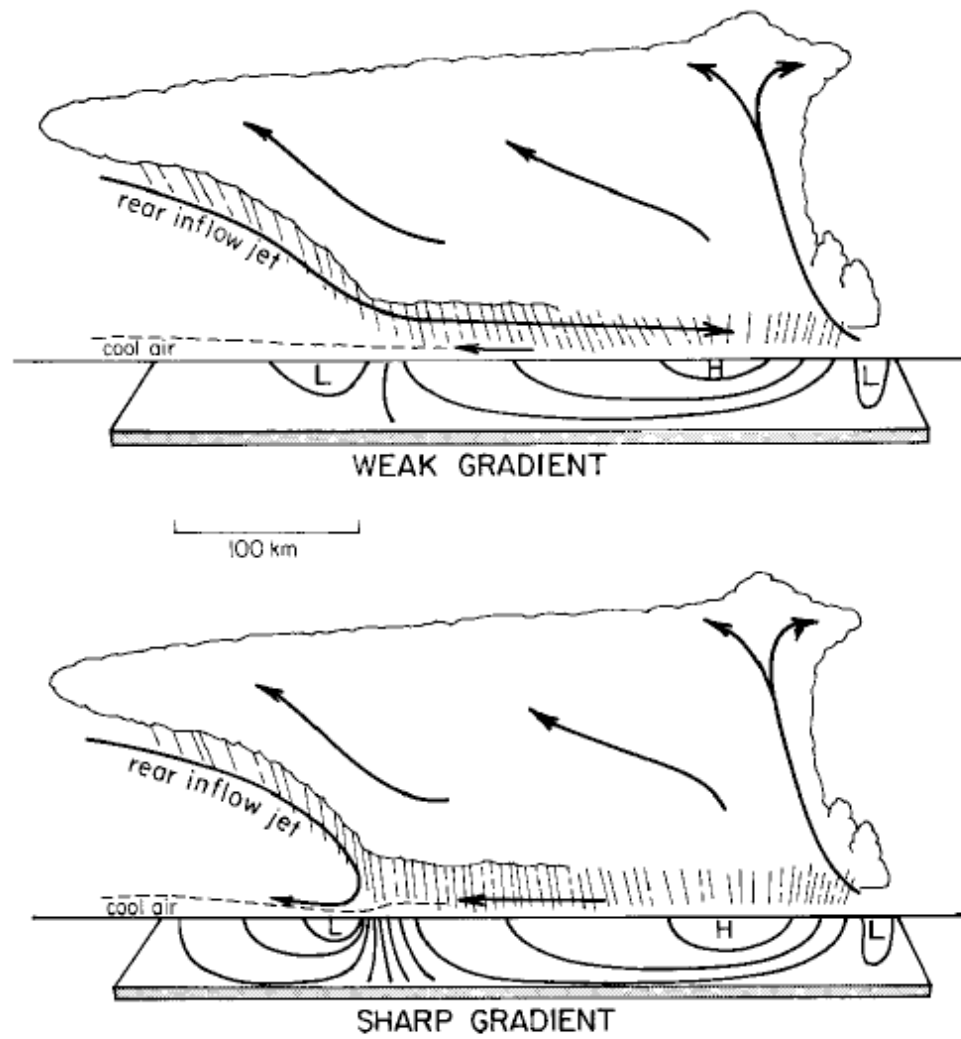


FIG. 16. Depiction of (top) weak and (bottom) sharp surface pressure gradients in association with rear-inflow jets that continue forward toward the leading convective line or are blocked, respectively.



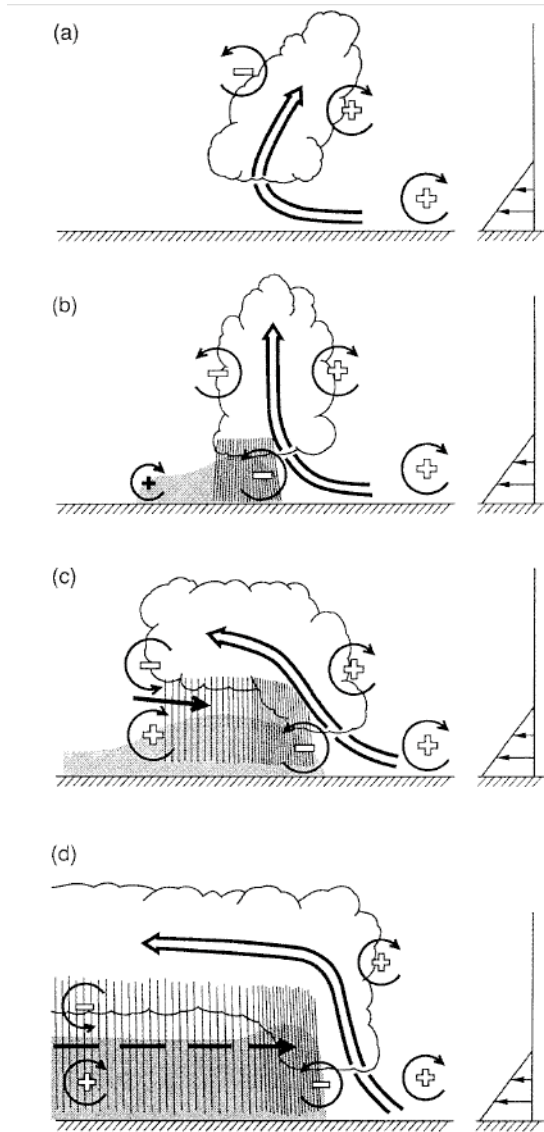


FIG. 23. Four stages in the evolution of an idealized bow echo developing in a strongly sheared, large-CAPE environment. The updraft current is denoted by the thick, double-lined flow vector, with the rear-inflow current in (c) denoted by the thick solid vector. The shading denotes the surface cold pool. The thin, circular arrows depict the most significant sources of horizontal vorticity, which are either associated with the ambient shear or which are generated within the convective system, as described in the text. Regions of lighter or heavier rainfall are indicated by the more sparsely or densely packed vertical lines, respectively. The scalloped line denotes the outline of the cloud. [From Weisman (1993).]

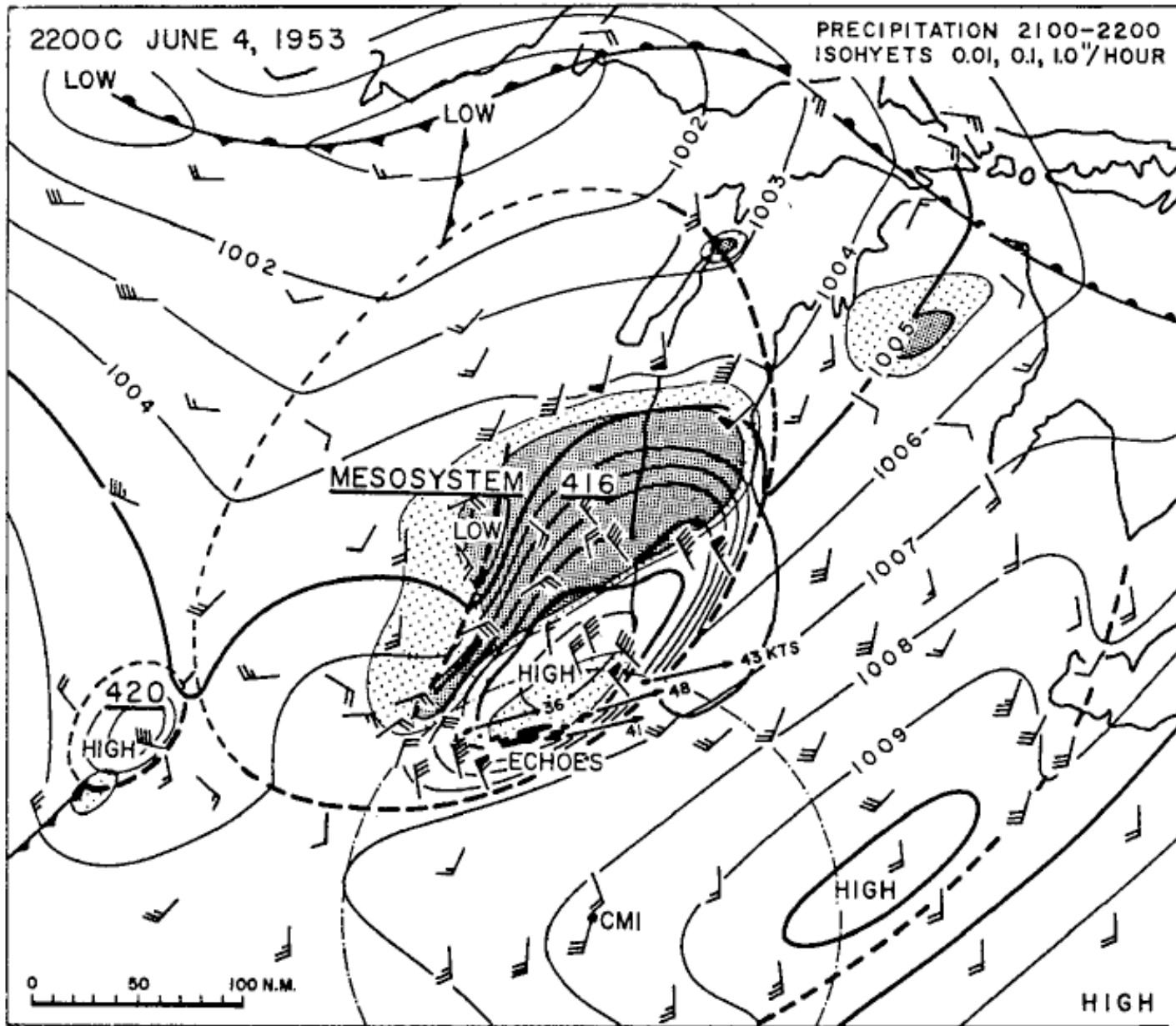


FIG. 8. Surface chart for 2200 CST 4 Jun 1953. From Fujita and Brown (1958). Johnson 2001

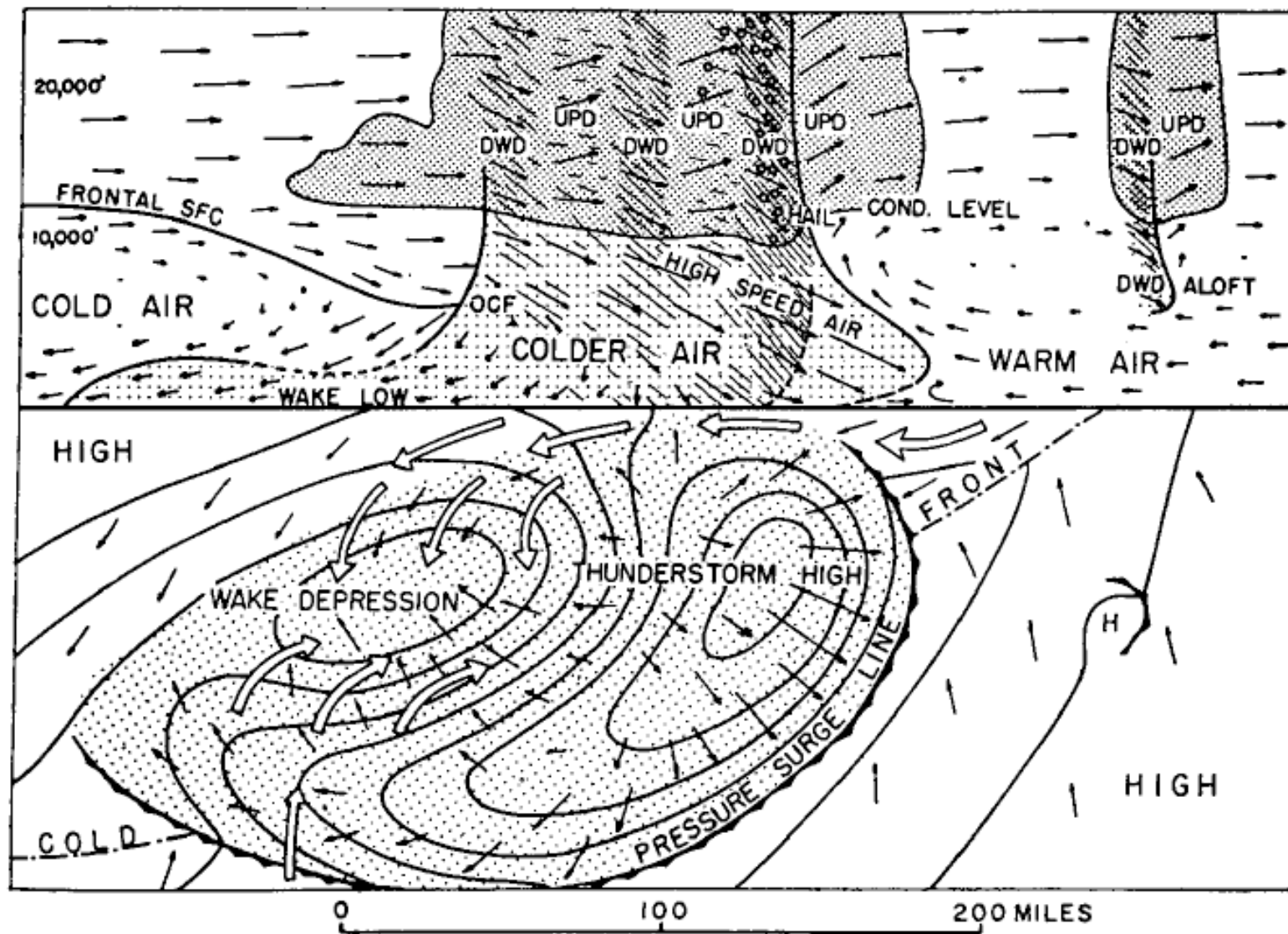
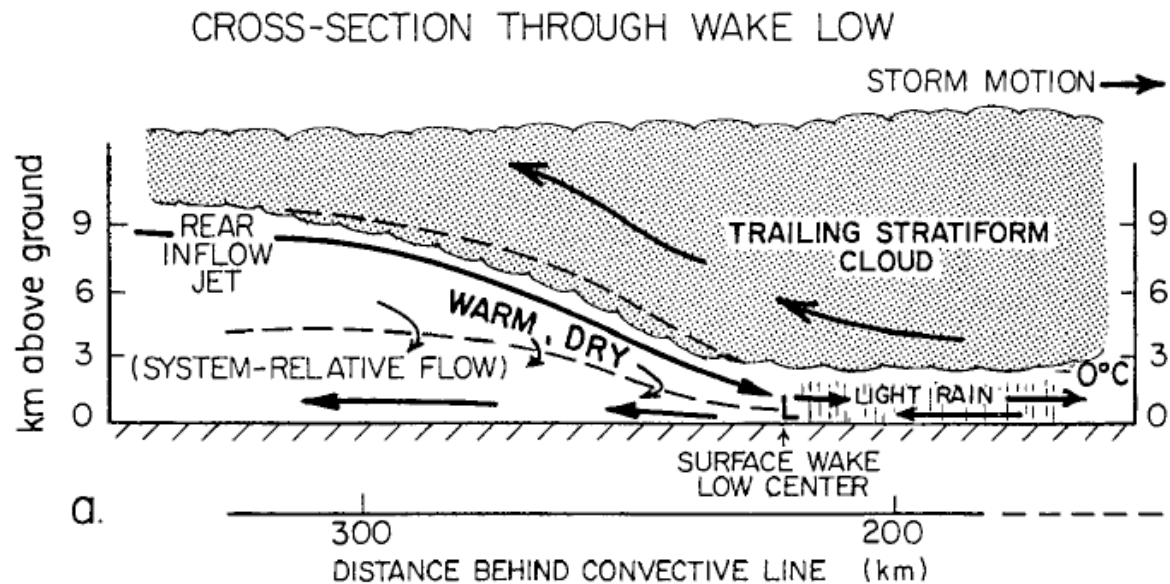


FIG. 4. Fujita's early model of squall-line circulation: DWD = downdraft, UPD = updraft. From Fujita (1955).

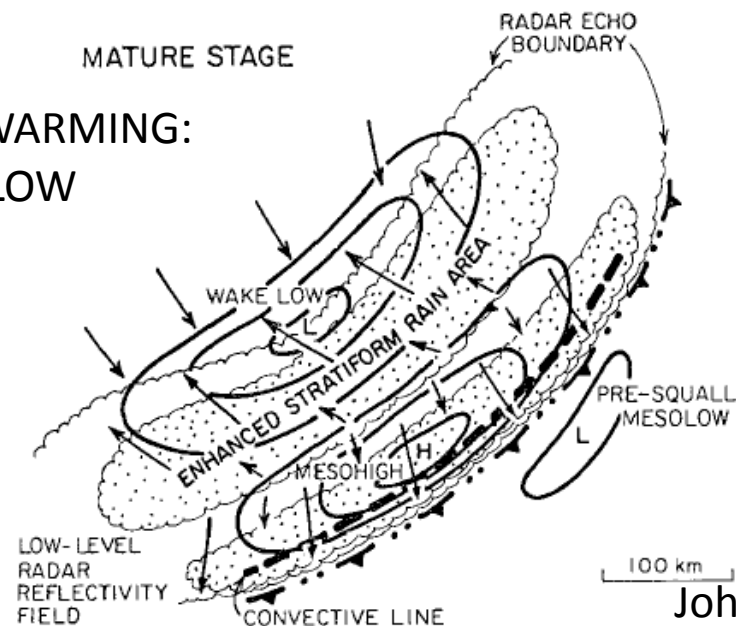
drometeor loading (Sanders and Emanuel 1977; Nicholls et al. 1988).

Since the first central and high plains surface mesonet network of Fujita's era in the early 1950s and the National Severe Storms Project  $\alpha$  network in the early 1960s (Fujita 1963), no network even approaching that one in areal coverage had been deployed until the 1985 Oklahoma-Kansas Preliminary Regional Experiment for STORM-Central (OK PRE-STORM). In this experiment 5-min data were col-



a.

### SUBSIDENCE WARMING: WAKE LOW



b.

Johnson 2001

FIG. 10. Schematic cross section through the wake low at the trailing edge of (a) a squall line and (b) surface pressure and wind fields and precipitation distribution during the squall-line mature stage. Winds in (a) are system relative with the dashed line denoting zero relative wind. Arrows indicate streamlines, not trajectories, with those in (b) representing actual winds. Note that horizontal scales differ in the two schemata. From Johnson and Hamilton (1988).



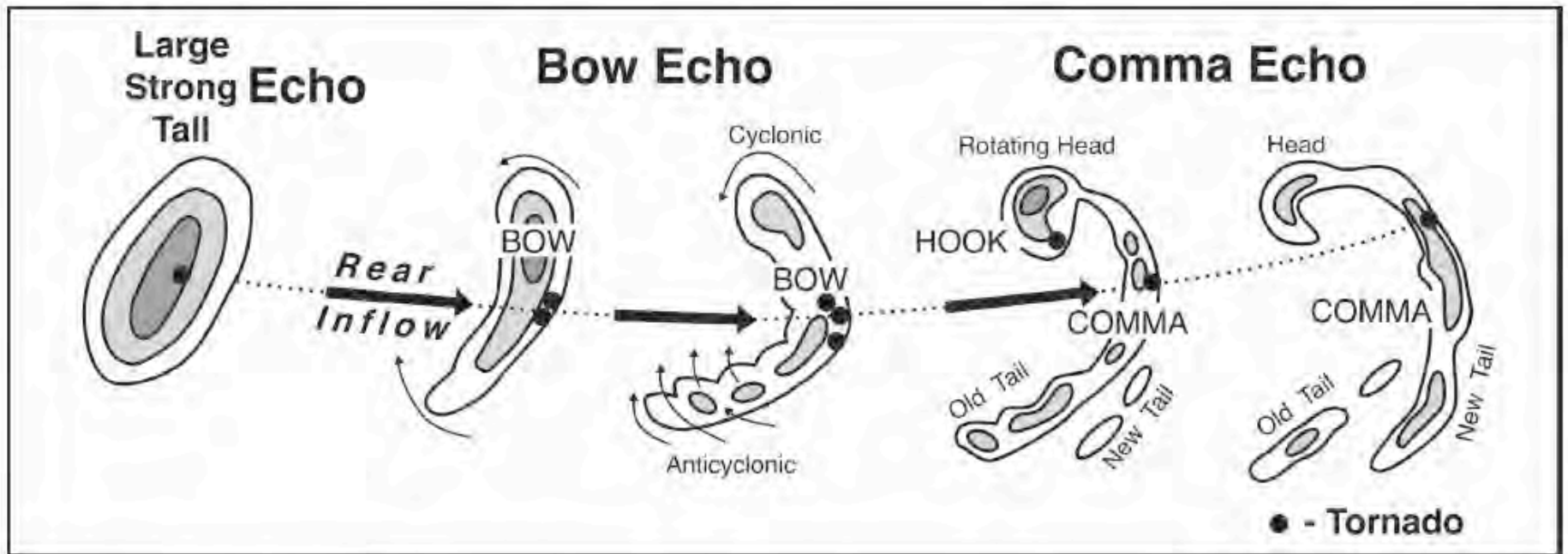


FIG. 1. Schematic diagram of the life cycle of a bow echo. Black arrows represent the approximate location of the rear-inflow jet. Black dots denote the location of tornadoes. Based on a figure from Fujita (1978).

Wakimoto et al. 2006

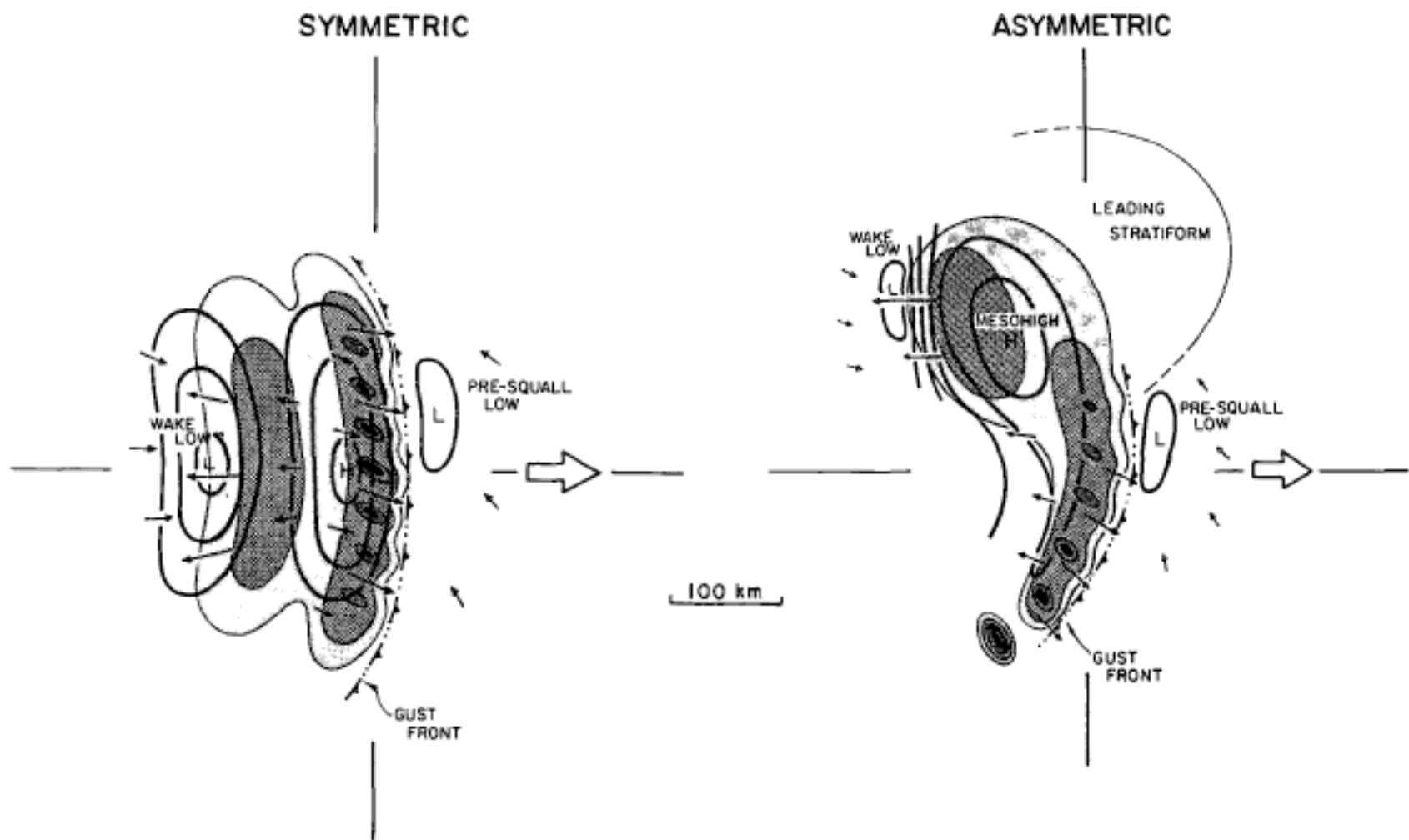


FIG. 22. Conceptual model of the surface pressure, flow, and precipitation fields associated with the (a) symmetric and (b) asymmetric stages of the MCS life cycle. Radar reflectivity field is adapted from Houze et al. (1990). Levels of shading denote increasing radar reflectivity, with darkest shading corresponding to convective cell cores. Pressure is in 1-mb increments. Small arrows represent the surface flow. Lengths of the arrows are proportional to the wind speed found at their center. The large arrows represent the storm motion with quadrants defined in Fig. 1 and text indicated.

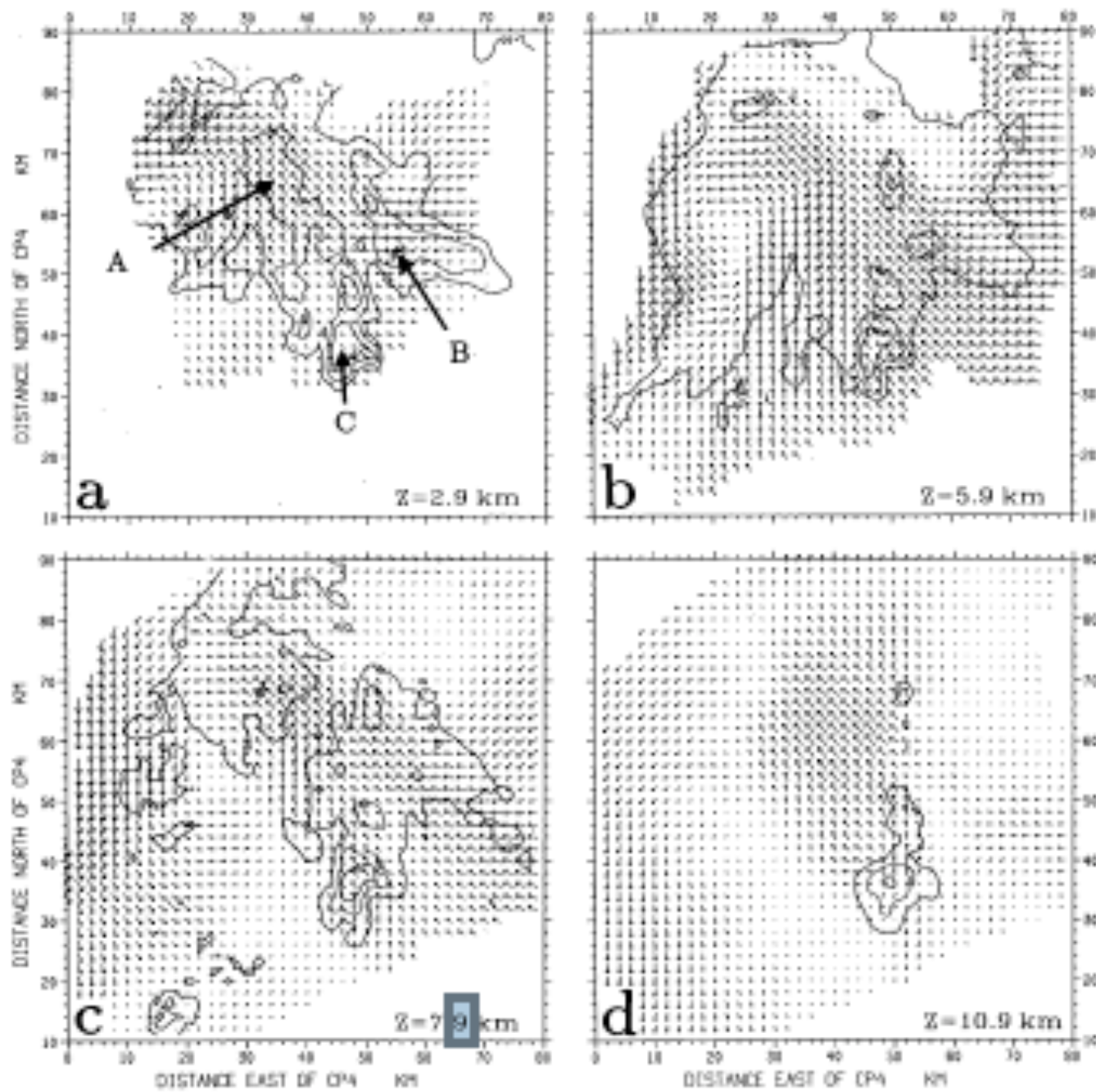


FIG. 7. Same as Fig. 6, only for 0140 UTC.



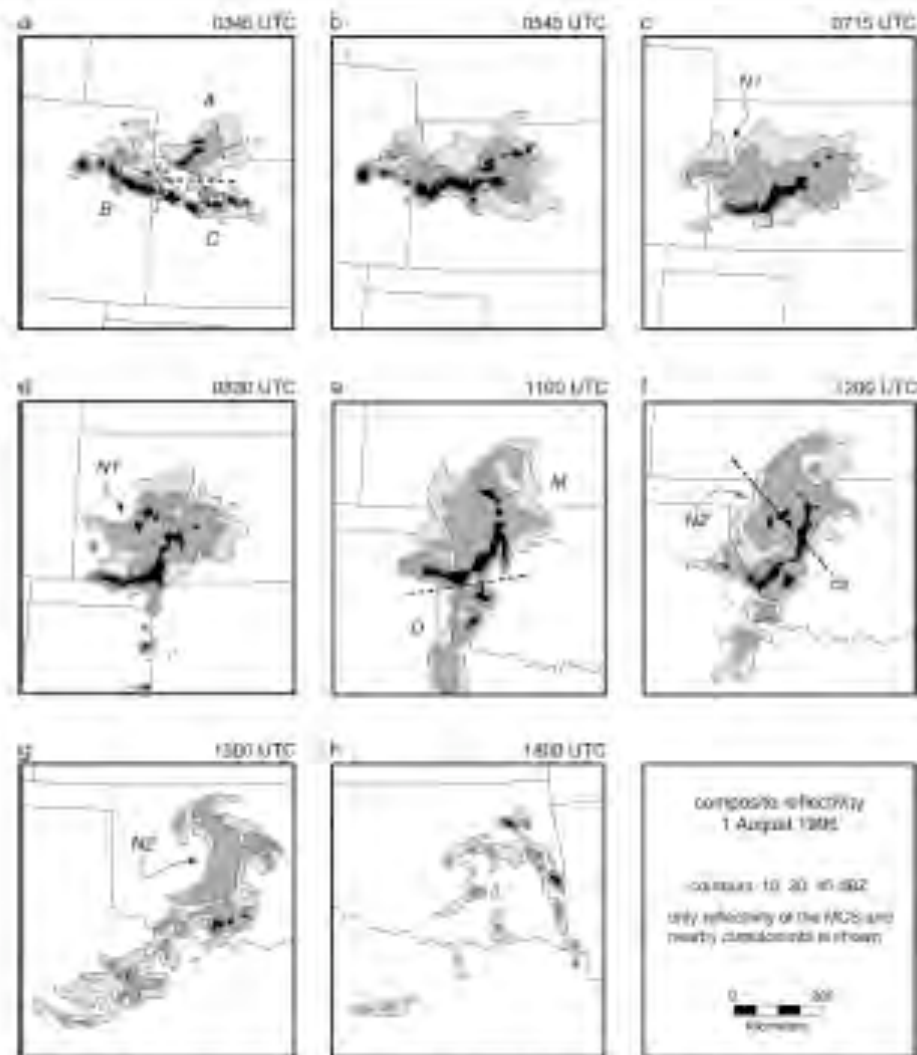


FIG. 2. Schemata of composite base-ten radar reflectivity on 1 Aug 1995. Times are (a) 0345, (b) 0545, (c) 0715, (d) 0830, (e) 1100, (f) 1200, (g) 1300, and (h) 1400 UTC. Contours are at 10, 20, and 45 dBZ. Only reflectivity due to the MCS and nearby convective cells is shown. Clusters that merged to form the MCS are separated by dashed lines and marked by A, B, and C. A head of mesocyclone overlain by the MCS, M, is marked by D; the two are separated by a dashed line. Noctua are marked by N1 and N2. The location of the cross section in Fig. 1b is marked by  $\alpha$ .

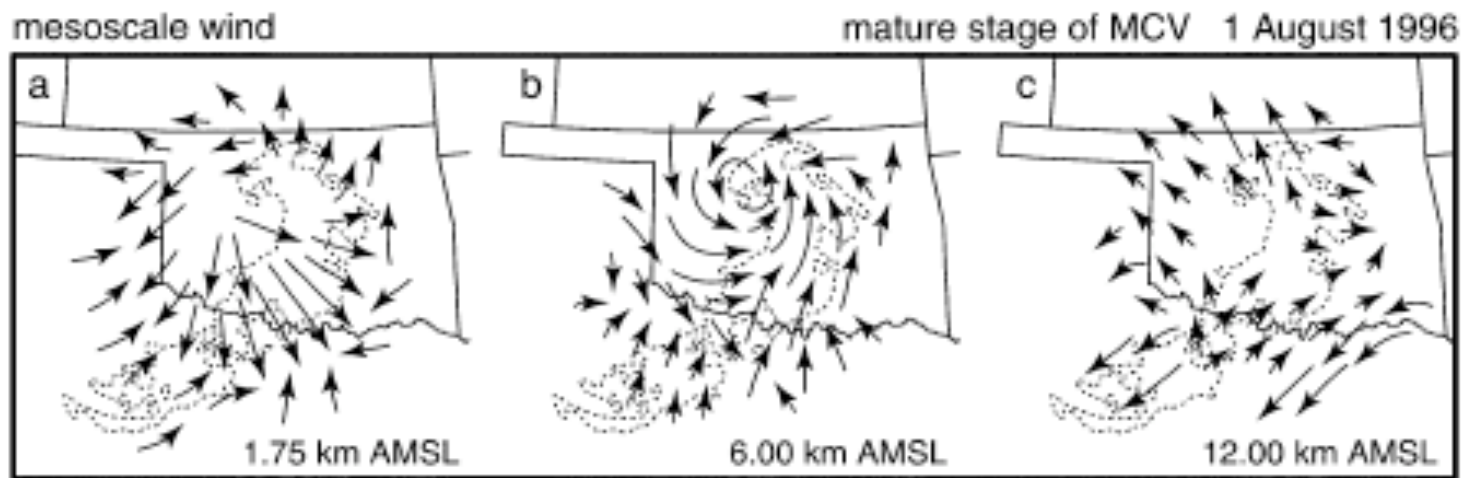


FIG. 14. Schemata of horizontal mesoscale perturbation in wind at 1500 UTC 1 Aug 1996. Altitudes are (a) 1.75, (b) 6.00, and (c) 12.00 km AMSL. Arrows are a hybrid of vectors and streamlines, and their lengths roughly indicate relative wind speed. The contour of 15 dBZ reflectivity within the MCS is dashed.

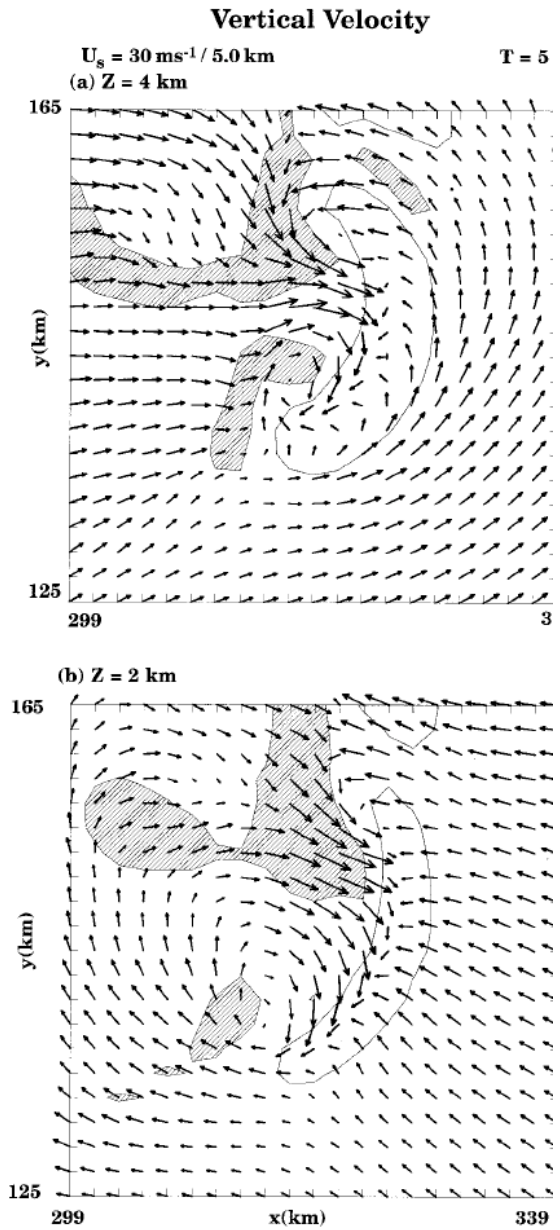
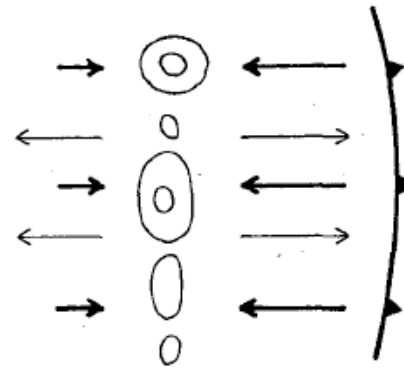


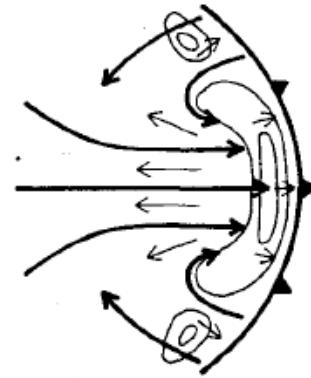
FIG. 21. Horizontal cross section of storm-relative winds and vertical velocity (shaded for greater than  $5 \text{ m s}^{-1}$  and cross hatched less than  $-2 \text{ m s}^{-1}$ ) at (a) 4 km and (b) 2 km AGL for the southernmost cell for the  $U_s = 30 \text{ m s}^{-1}$  simulation at 5 h. A domain speed of  $u_m = 18.5 \text{ m s}^{-1}$  has been subtracted from the flow field. T marks are spaced at 10-km intervals.

“BOOKEND VORTICES”  
 (“LINE-END VORTICES”)  
 $\geq 20 \text{ m s}^{-1}$  SHEAR, LOWEST 2.5 – 5 km

a) Weak Cells  
 (“W”)



b) Bow Echo  
 (“B”)



c) Split Cells  
 (“S”)

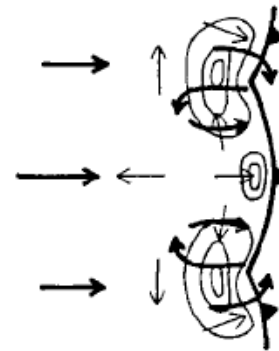


FIG. 23. Schematic depiction of the primary modes of convective organization identified in the sensitivity experiments between 180 and 240 min. Thick and thin arrows represent system-relative flow at 2.5 km AGL and the surface, respectively. Contours represent rainwater concentration. Thick barbed line represents the location of the surface gust front.

Weisman 1993

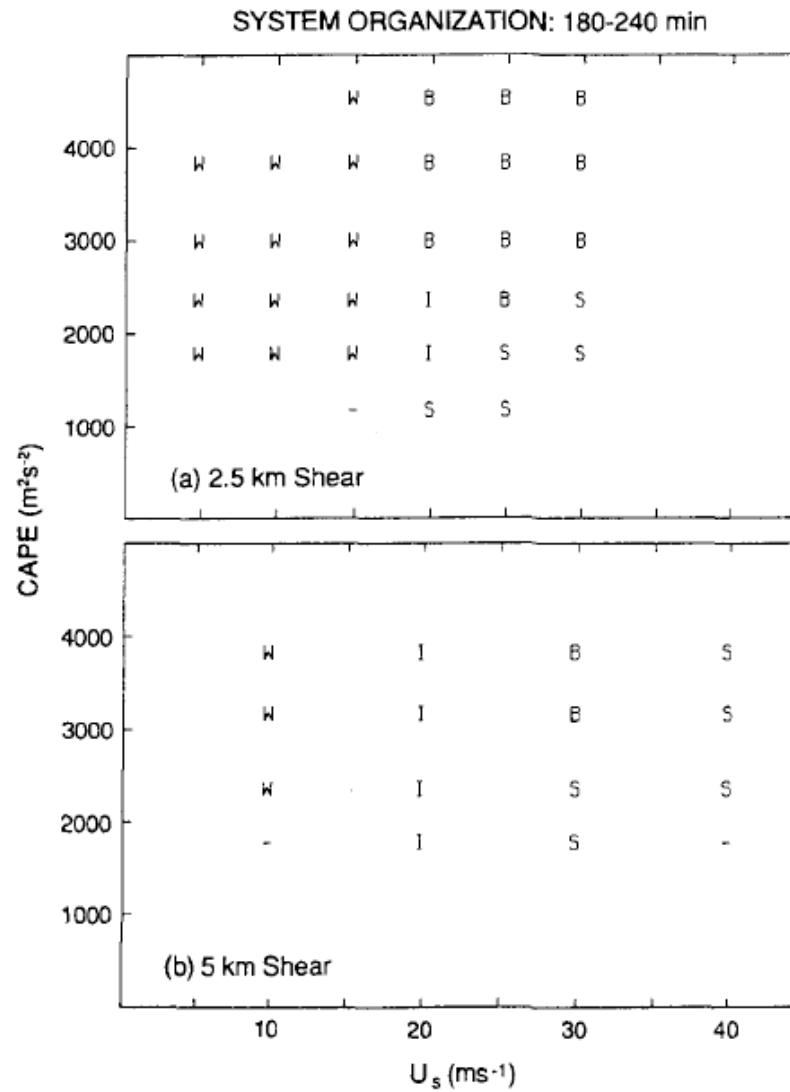


FIG. 24. Primary modes of convective organization identified for the (a) 2.5-km shear and (b) 5-km shear experiments between 180 and 240 min for each simulation.  $U_s$  represents the maximum magnitude of the wind for each wind profile. In the figure W represents a weak upshear-tilted system, I represents an intermediate form of organization, B represents a bow echo, and S represents split supercells, as described in Fig. 23 and in the text; “-” indicates that the storm system had dissipated by 180 min.

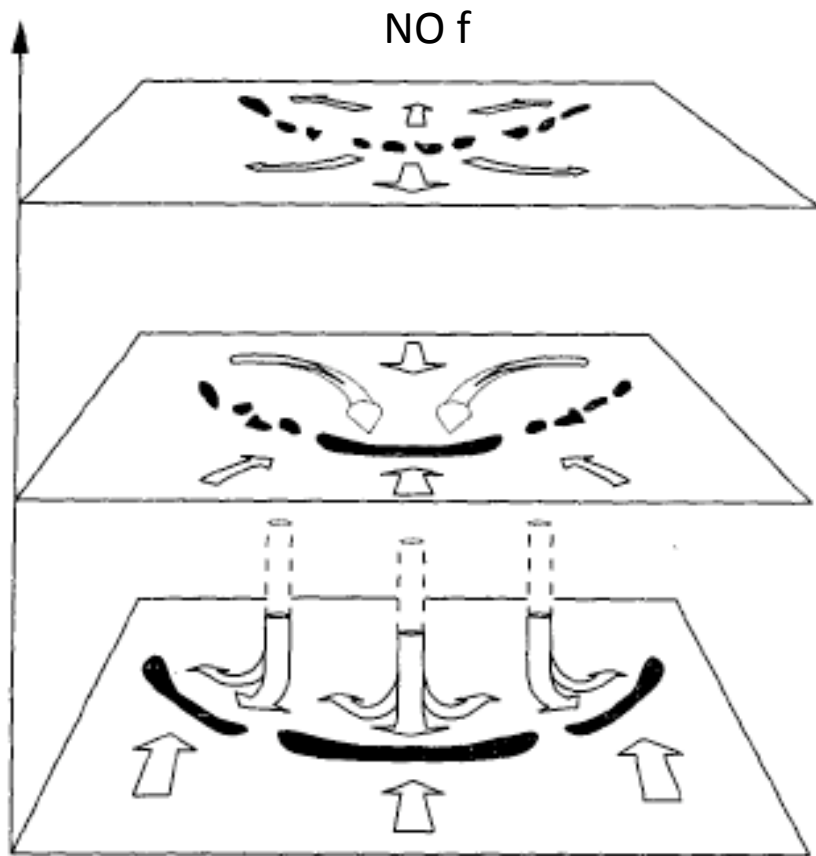


FIG. 23. Conceptual model of the mature line that has evolved without Coriolis forcing. The view is looking down from the east. The planes represent surface, mid-, and upper-level cross sections. 2D arrows denote flow in the plane and 3D tubes denote flow out of the plane. The dotted tubes depicted descending flow. The dark stippling denotes regions of updrafts and active convection.

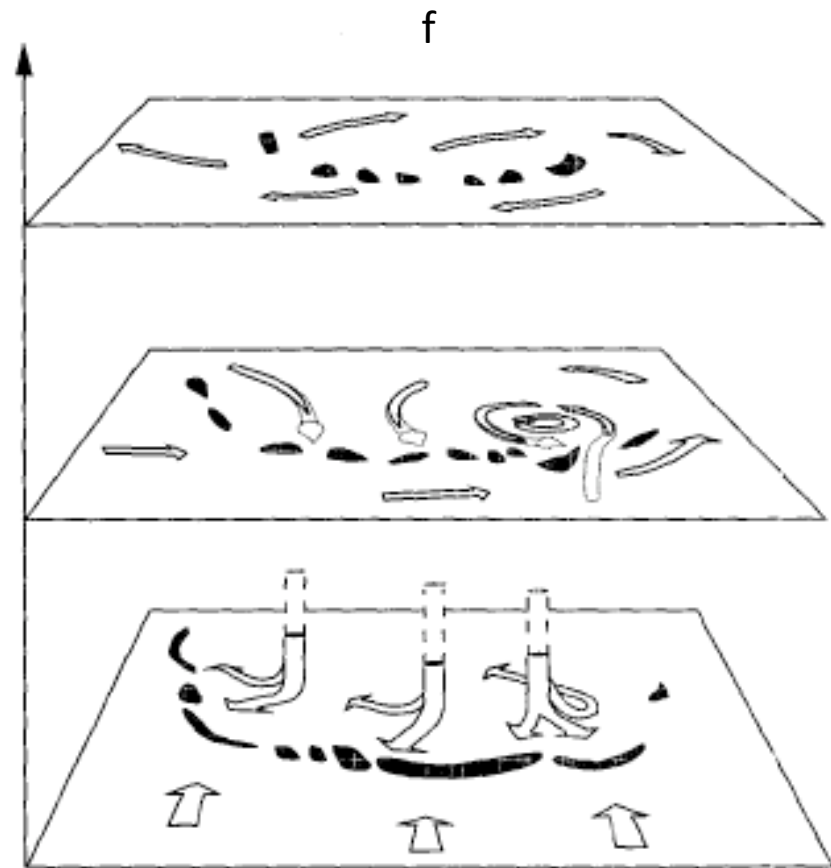
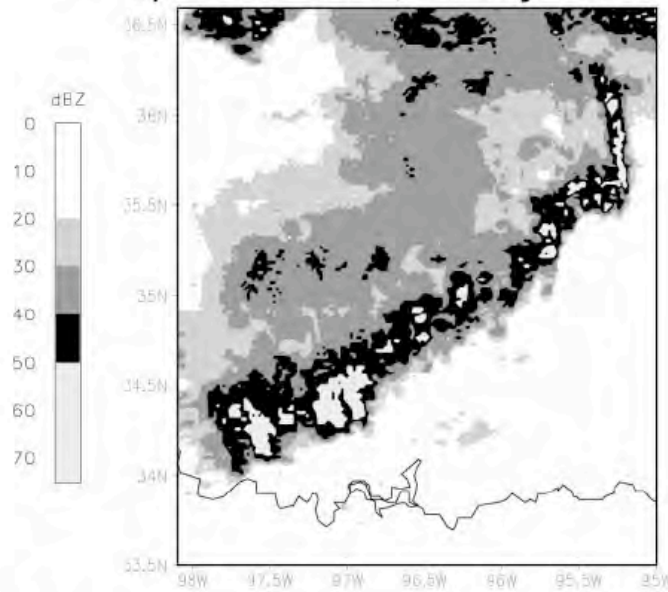


FIG. 24. Conceptual model of the mature line that has evolved with Coriolis forcing, rendered as in Fig. 23.

a) 0700 UTC, 8 May 1997



TRAILING STRATIFORM

b) 0200 UTC, 23 May 1997 c) 0200 UTC, 24 May 1997

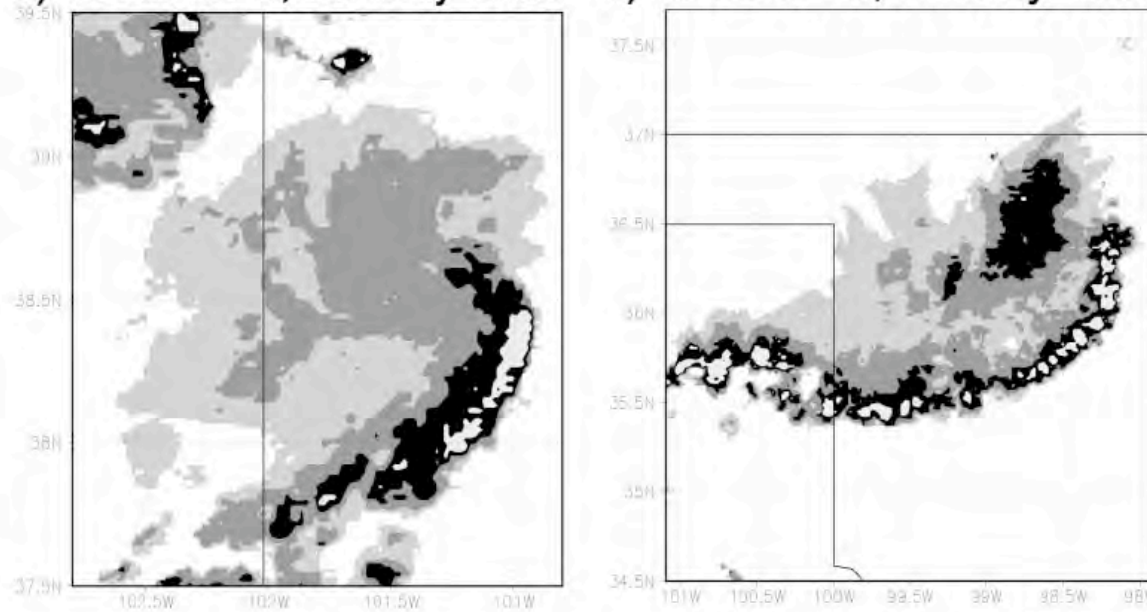
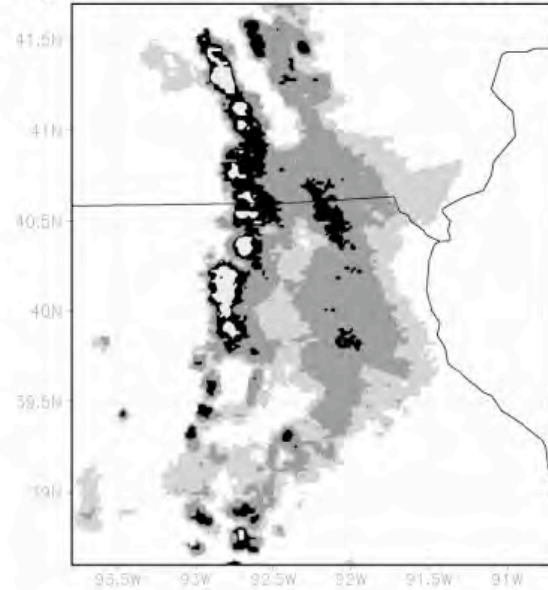


FIG. 5. Radar reflectivity—examples for TS archetype: (a) 0700 UTC 8 May 1997, (b) 0200 UTC 23 May 1997, and (c) 0200 UTC 24 May 1997.

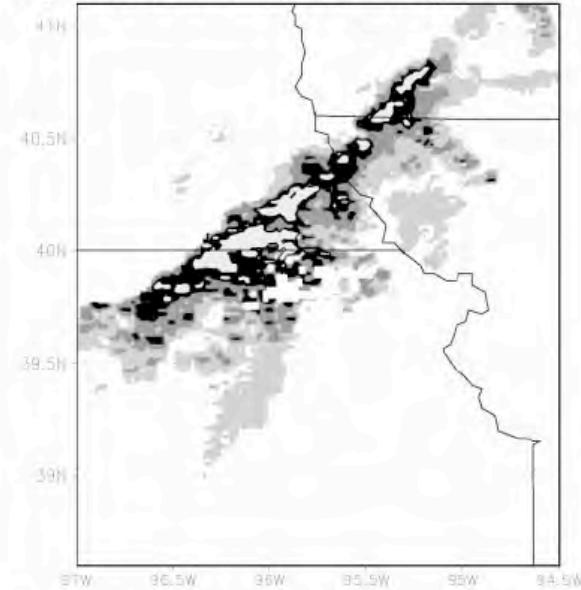
Parker and  
Johnson 2000



a) 1100 UTC, 18 May 1997

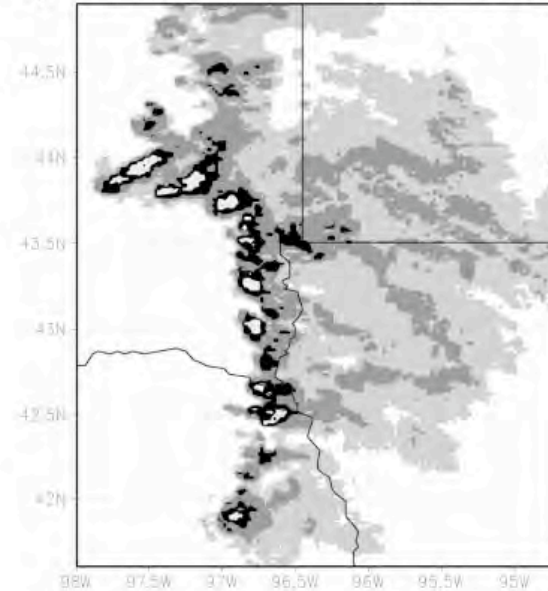


b) 0500 UTC, 18 May 1996

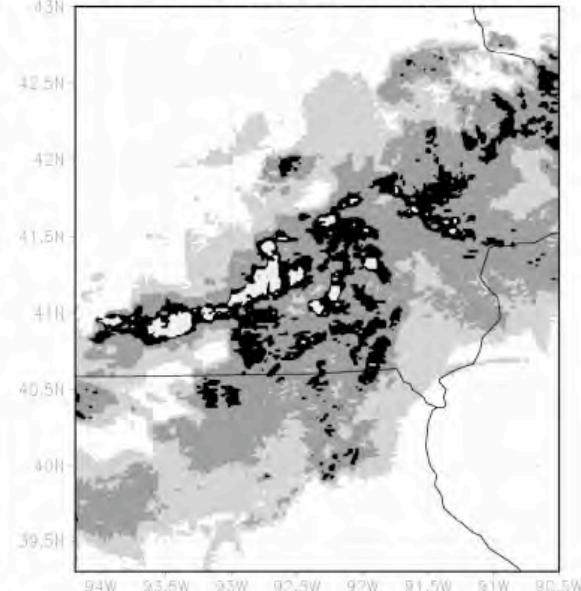


LEADING  
STRATIFORM

c) 1100 UTC, 7 May 1997



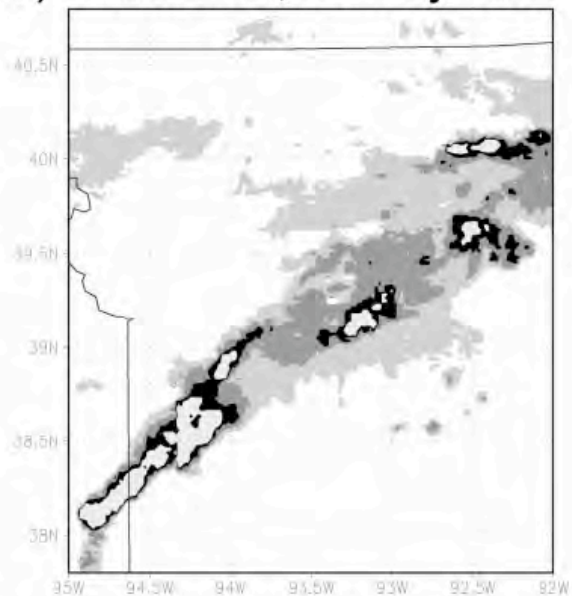
d) 0100 UTC, 8 May 1997



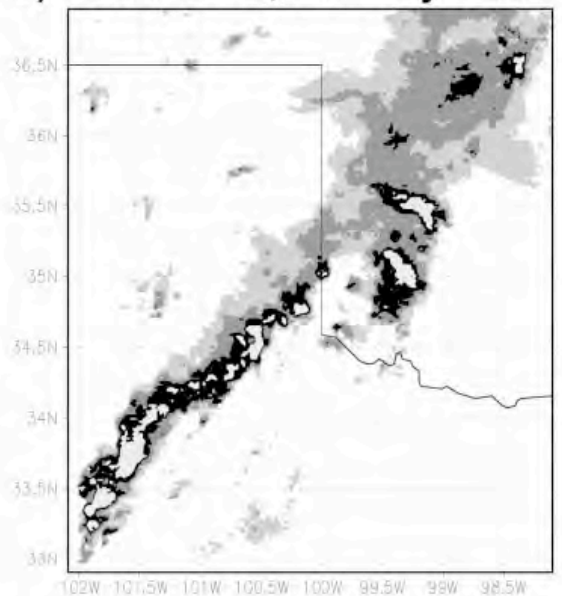
Parker and  
Johnson 2000

FIG. 6. Radar reflectivity—examples for LS archetype: (a) 1100 UTC 18 May 1997, (b) 0500 UTC 18 May 1996, (c) 1100 UTC 7 May 1997, and (d) 0100 UTC 8 May 1997. Reflectivities shaded as in Fig. 5.

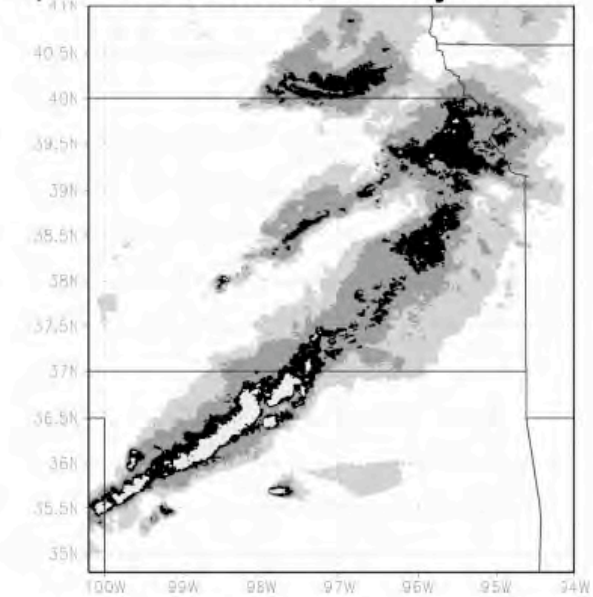
a) 2100 UTC, 24 May 1996



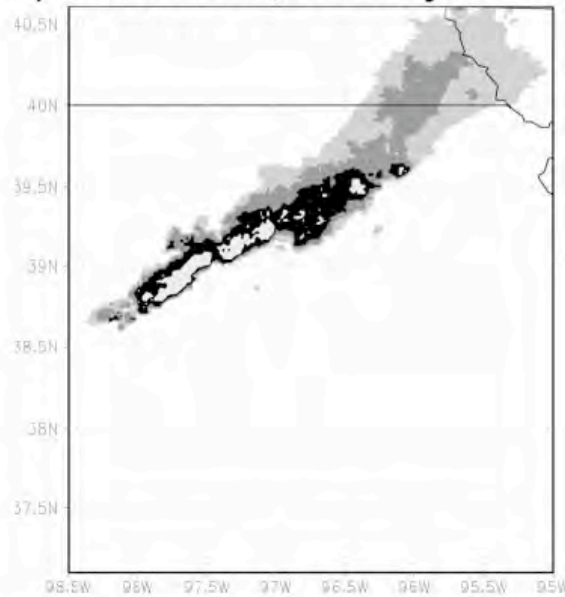
b) 1000 UTC, 26 May 1996



c) 0400 UTC, 2 May 1997



d) 0500 UTC, 24 May 1997



PARALLEL  
STRATIFORM

FIG. 7. Radar reflectivity—examples for PS archetype: (a) 2100 UTC 24 May 1996, (b) 1000 UTC 26 May 1996, (c) 0400 UTC 2 May 1997, and (d) 0500 UTC 24 May 1997. Reflectivities shaded as in Fig. 5.

Parker and  
Johnson 2000

# Linear MCS archetypes

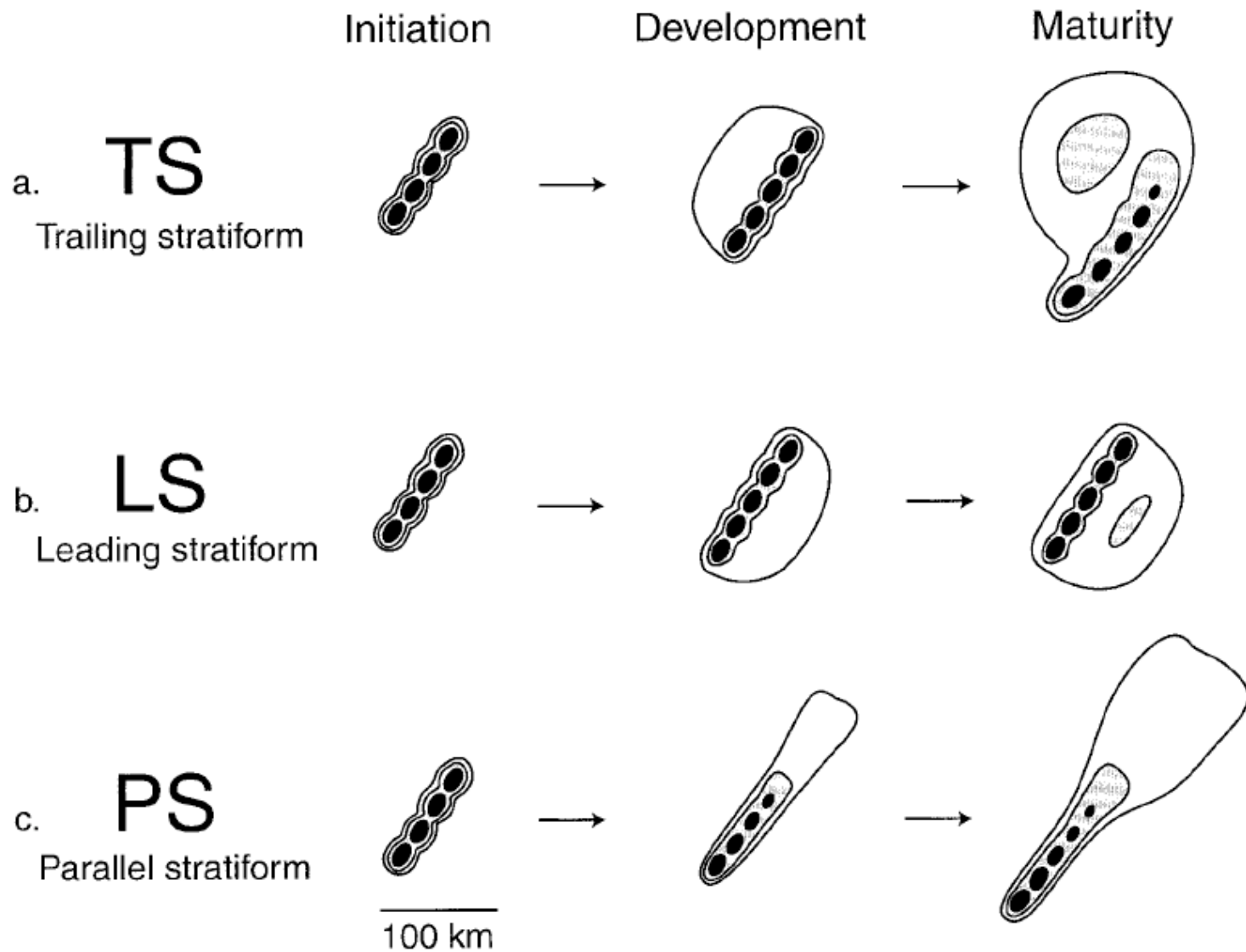


FIG. 4. Schematic reflectivity drawing of idealized life cycles for three linear MCS archetypes: (a) TS, (b) LS, and (c) PS. Approximate time intervals between phases: for TS 3–4 h; for LS 2–3 h; for PS 2–3 h. Levels of shading roughly correspond to 20, 40, and 50 dBZ.

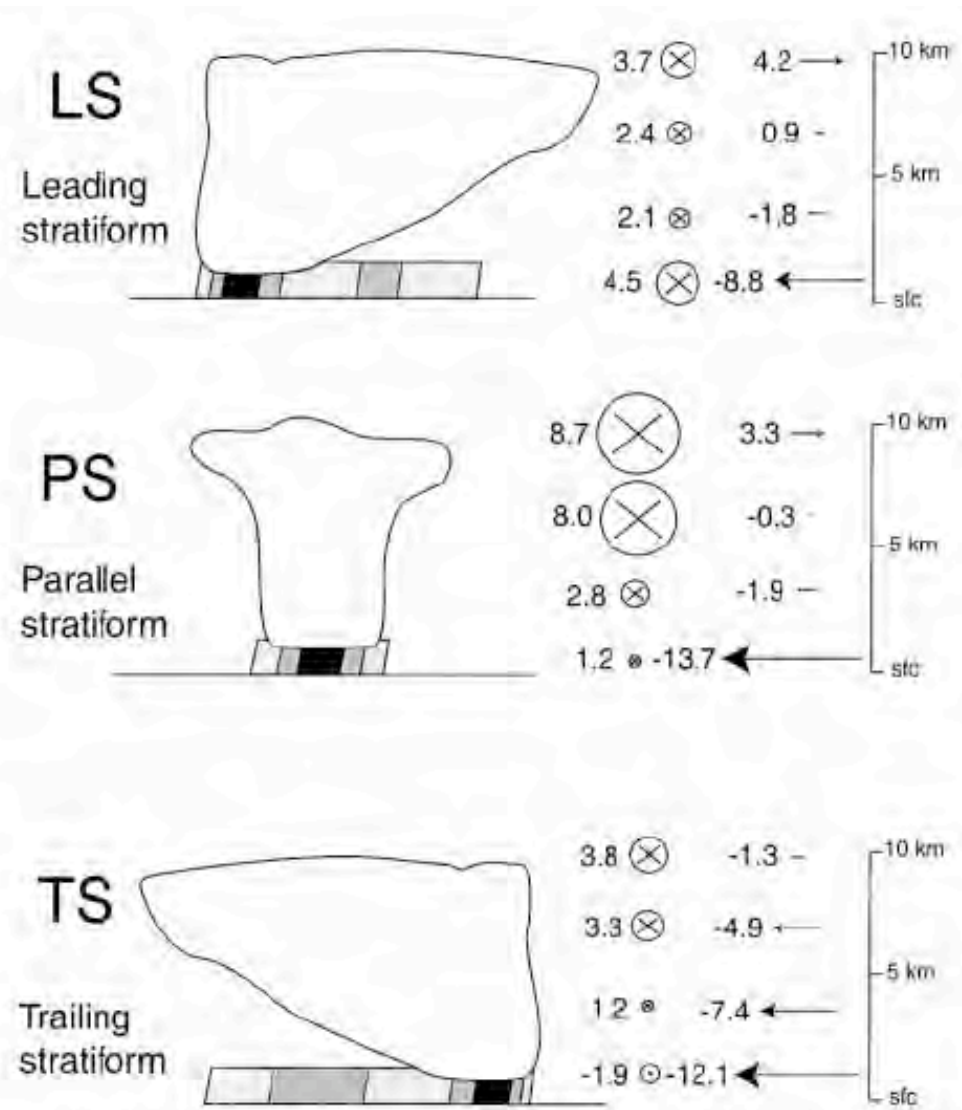


FIG. 12. Vertical profiles of layer-mean storm-relative pre-MCS winds for linear MCS classes. Wind vectors depicted as line-parallel (⊗) and line-perpendicular (→) components in  $m s^{-1}$ . Layers depicted are 0-1, 2-4, 5-8, and 9-10 km. Typical base scan radar reflectivity patterns (shading) and hypothetical cloud outlines are drawn schematically for reference. MCSs' leading edges are to the right.

Parker and Johnson  
2000

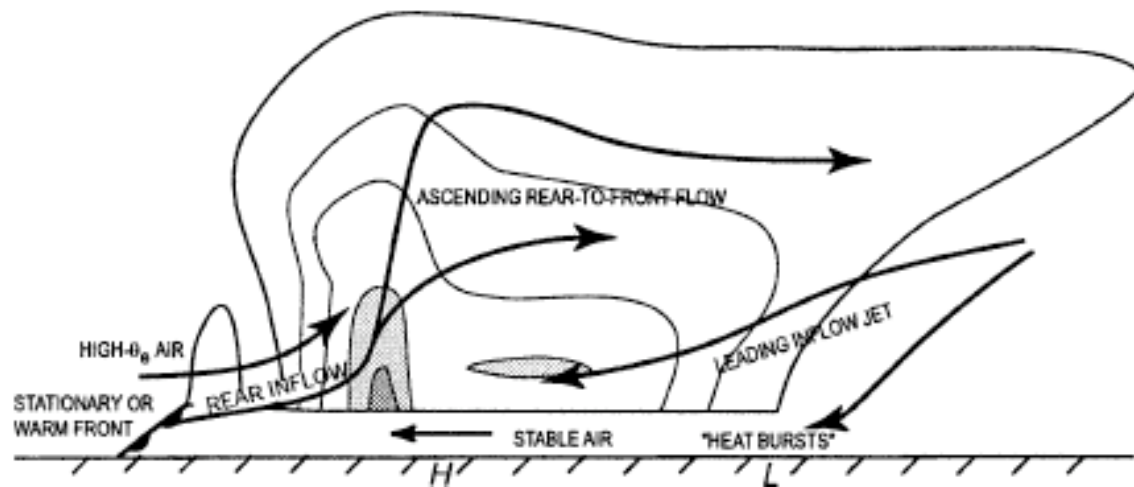


FIG. 5. Conceptual model, from Pettet and Johnson (2003), of a rear-fed convective line with leading precipitation, viewed in a vertical cross section oriented perpendicular to the convective line and parallel to its motion.



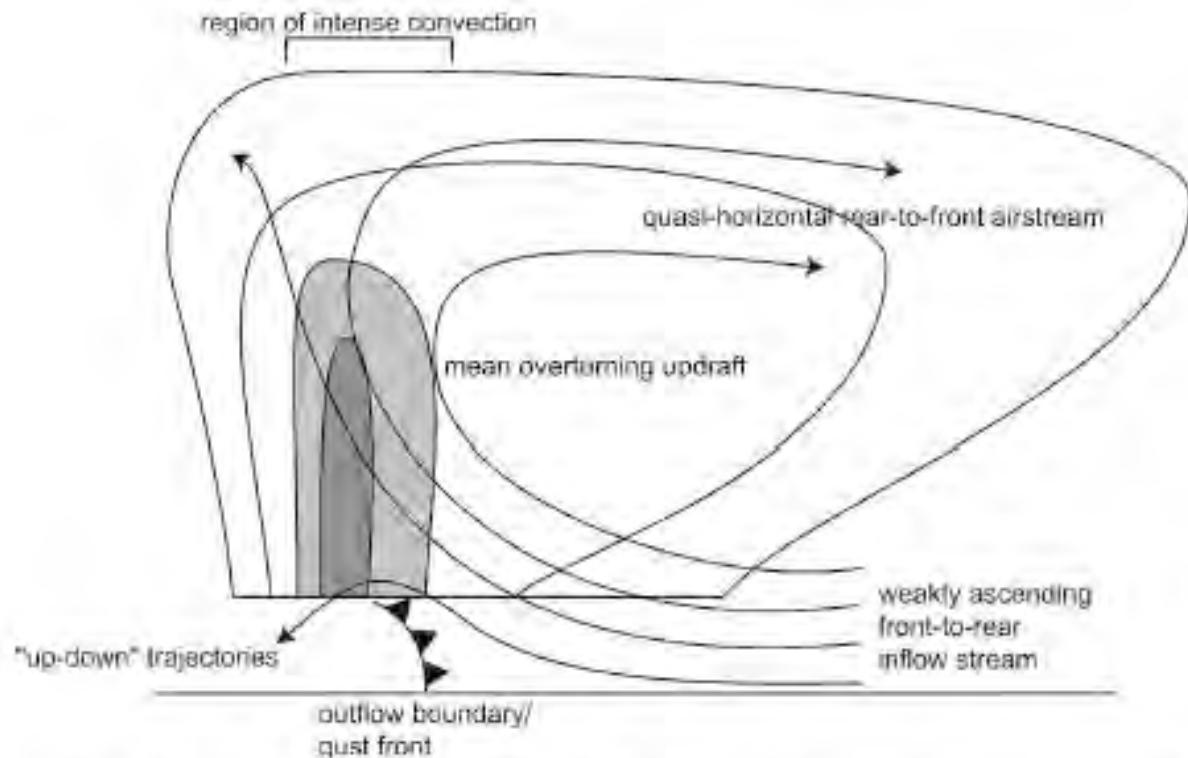


FIG. 1. Conceptual model of a front-fed convective line with leading precipitation, viewed in a vertical cross section oriented perpendicular to the convective line and parallel to its motion (PJ04c).

Storm et al. 2007



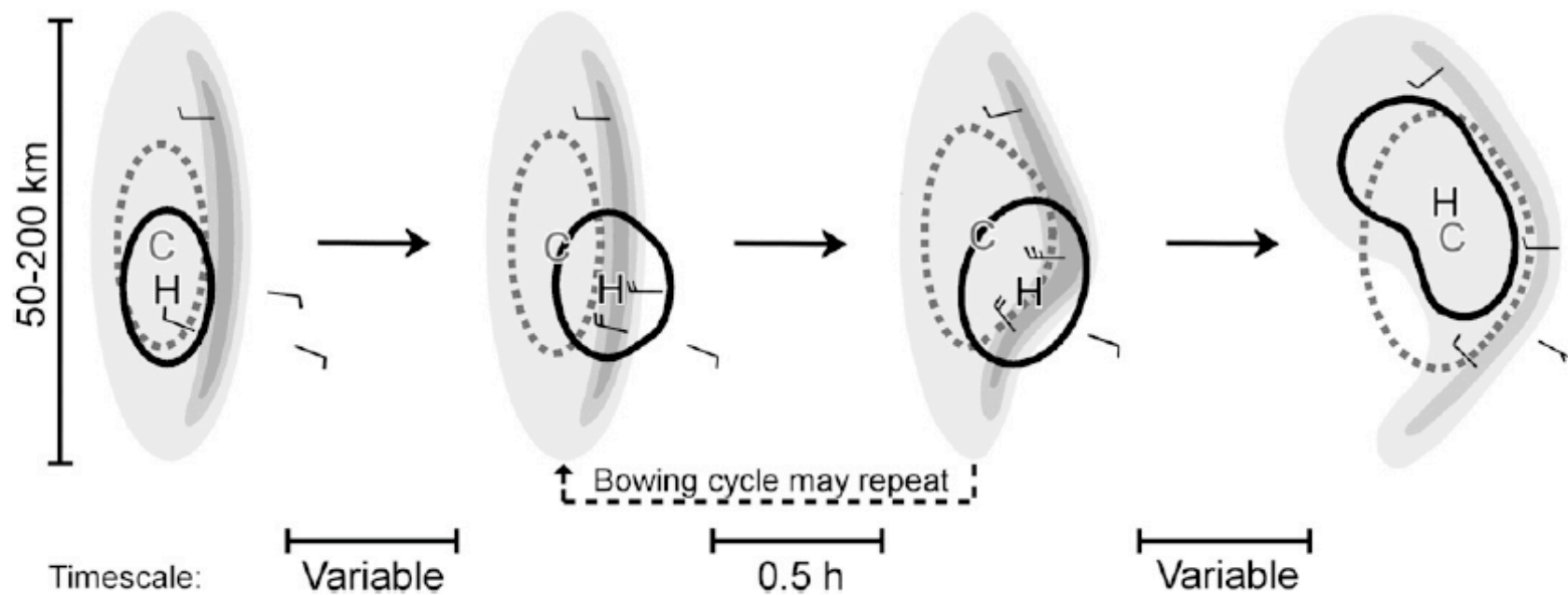


FIG. 7. Conceptual model for stages 1–4 of the relationship between pressure surge and new bowing. Shading roughly corresponds to radar reflectivity levels of 20, 40, and 50 dBZ. The dashed gray (solid black) contour surrounds the cold pool (mesohigh); C (H) is the point of lowest (highest) temperature (pressure) perturbation. Frequently observed surface winds and length and time scales are noted. Stages of development are the initial formation of convective line (stage 1), pressure surge ahead of convective line (stage 2), period of new bowing (stage 3), and dissipation (stage 4).

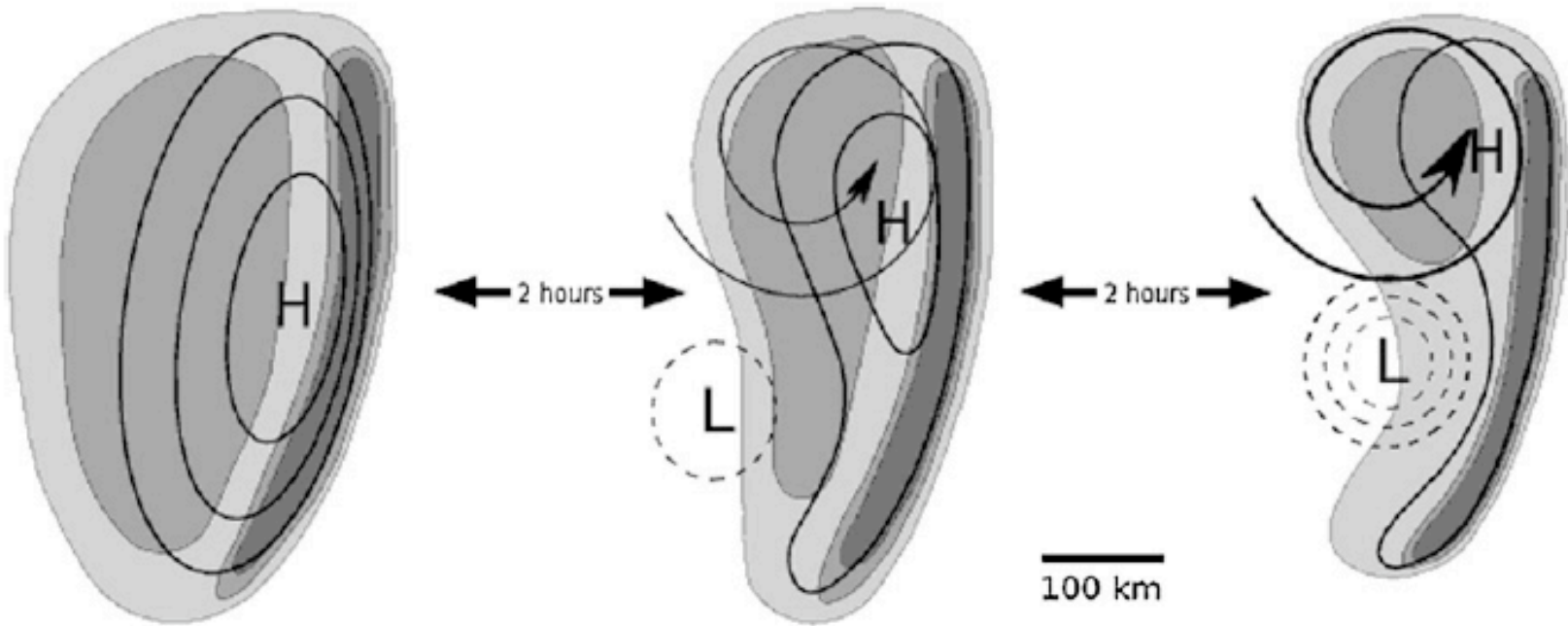


FIG. 20. Conceptual model of the typical evolution of a rear-inflow-jet MCV. Time runs from left to right, and evolution is with respect to a system moving toward the right. Shading represents composite radar reflectivity; light shading indicates 30–40 dBZ, moderate shading indicates 40–50 dBZ, and dark shading indicates >50 dBZ. Thin black lines represent isobars of surface pressure perturbation (contour interval 1 hPa; negative contours dashed). “H” indicates the center of the mesohigh, and “L” indicates the center of the mesolow. The spiral indicates the location of the developing midlevel vortex, with line thickness proportional to vortex intensity.

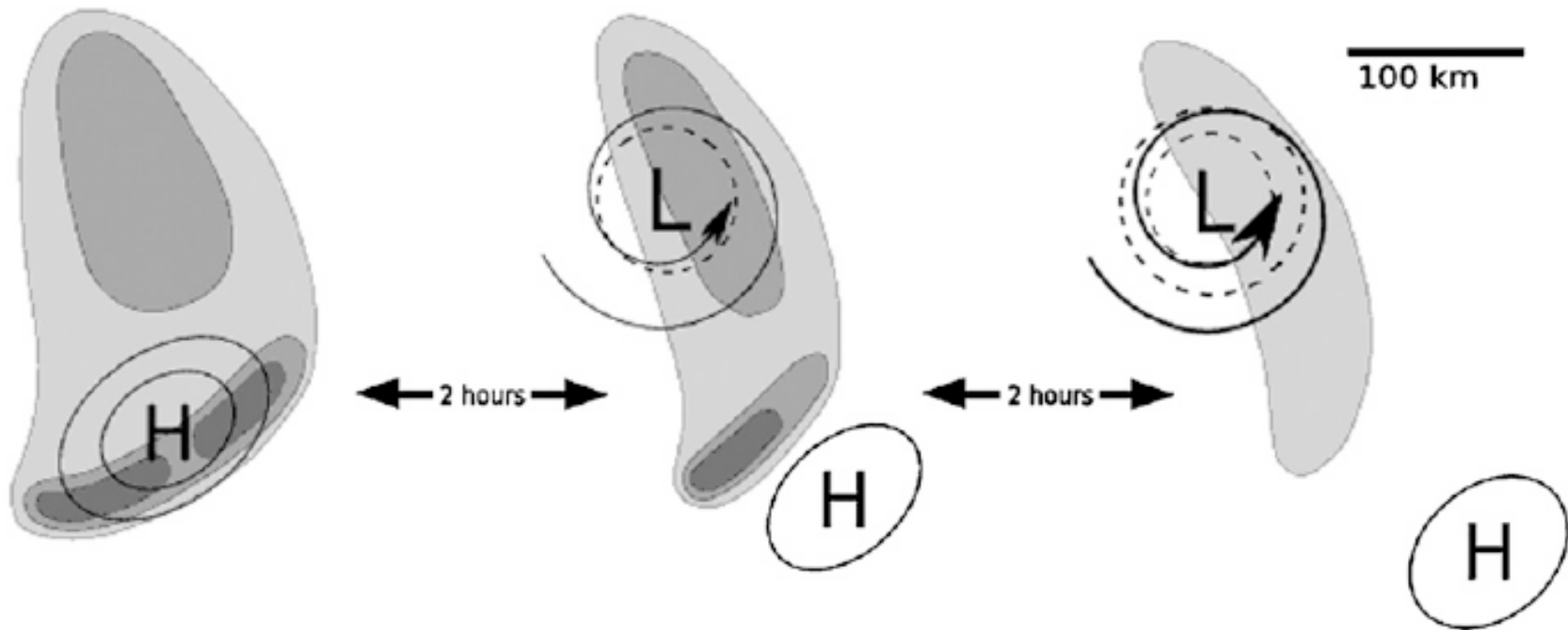


FIG. 21. As in Fig. 20, but of a collapsing-stratiform-region MCV.

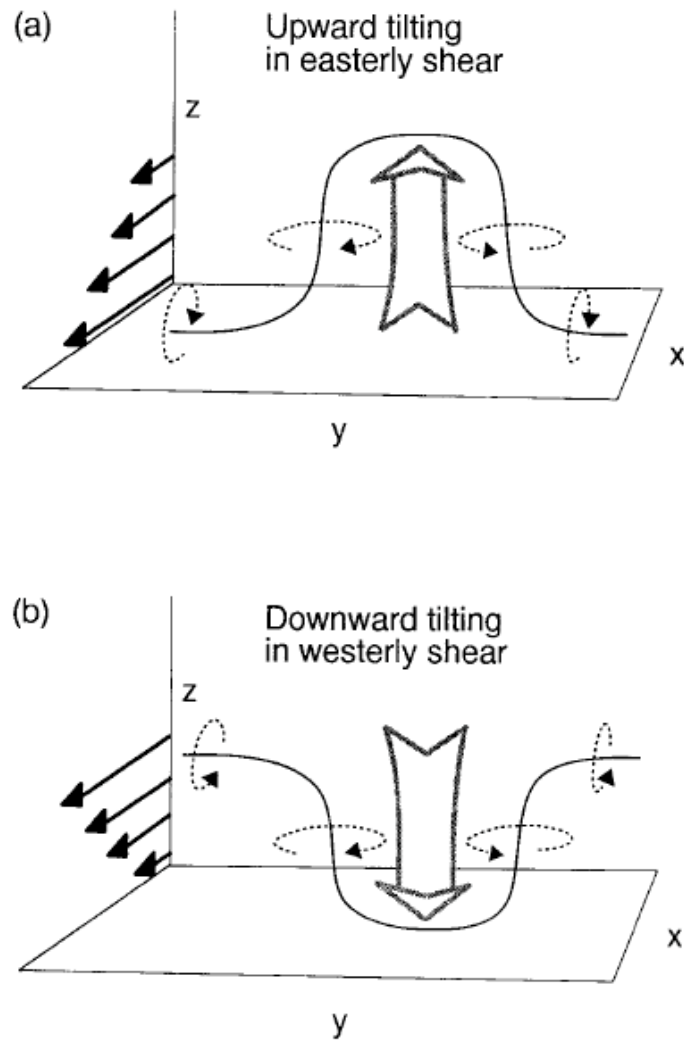


FIG. 24. Schematic of vertical vorticity generation through vortex tilting within finite convective lines and bow echoes. For (a) easterly shear, ascending motion within the central core of a line or bow echo pushes the vortex lines up, resulting in cyclonic rotation on the north end and anticyclonic rotation on the south end of the system. Localized descent in (b) westerly shear produces the same vertical vorticity pattern. [From Weisman and Davis (1998).]

Weisman 2001

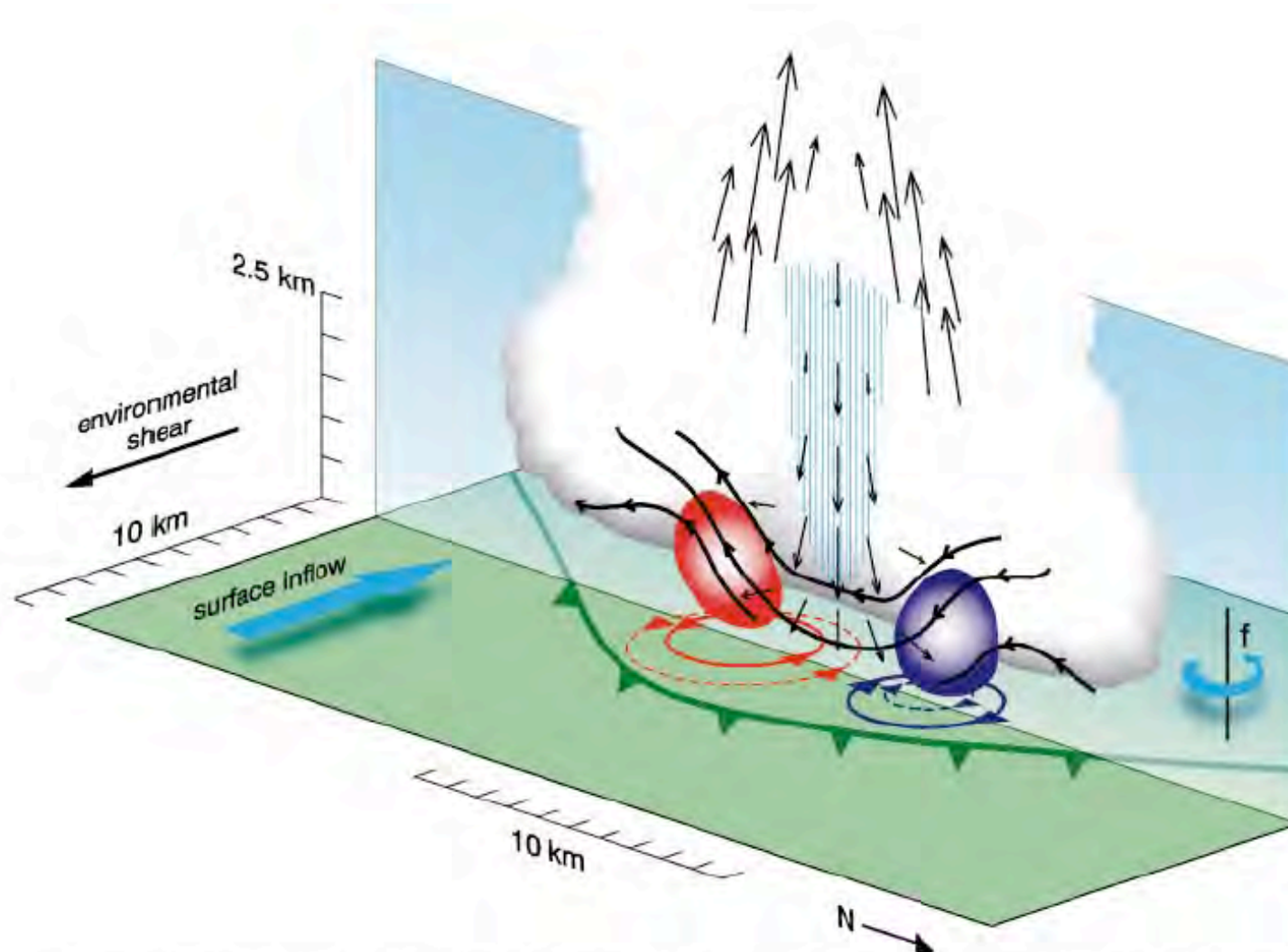


FIG. 23. Schematic showing a proposed mechanism for low-level mesovortexgenesis within a QLCS. The green barbed line indicates the gust front, vectors are of air motion in the vertical plane, blue hatching depicts rain core, bold black lines are vortex lines in the vertical plane, and red (purple) areas indicate positive (negative) vertical vorticity in the vertical plane. Vortex lines are tilted vertically by the downdraft, resulting in a surface vortex couplet (red is cyclonic vortex; purple is anticyclonic vortex). The future state of the vortex couplet, which results in part from the stretching of planetary vorticity ( $f$ ), is shown by the dashed red and purple circles. Schematic represents early-QLCS-stage vortexgenesis. During the mature QLCS stage, relevant vortex lines would have opposite orientation; hence, resultant vortex couplet orientation would be reversed.

Trapp and Weisman 1993



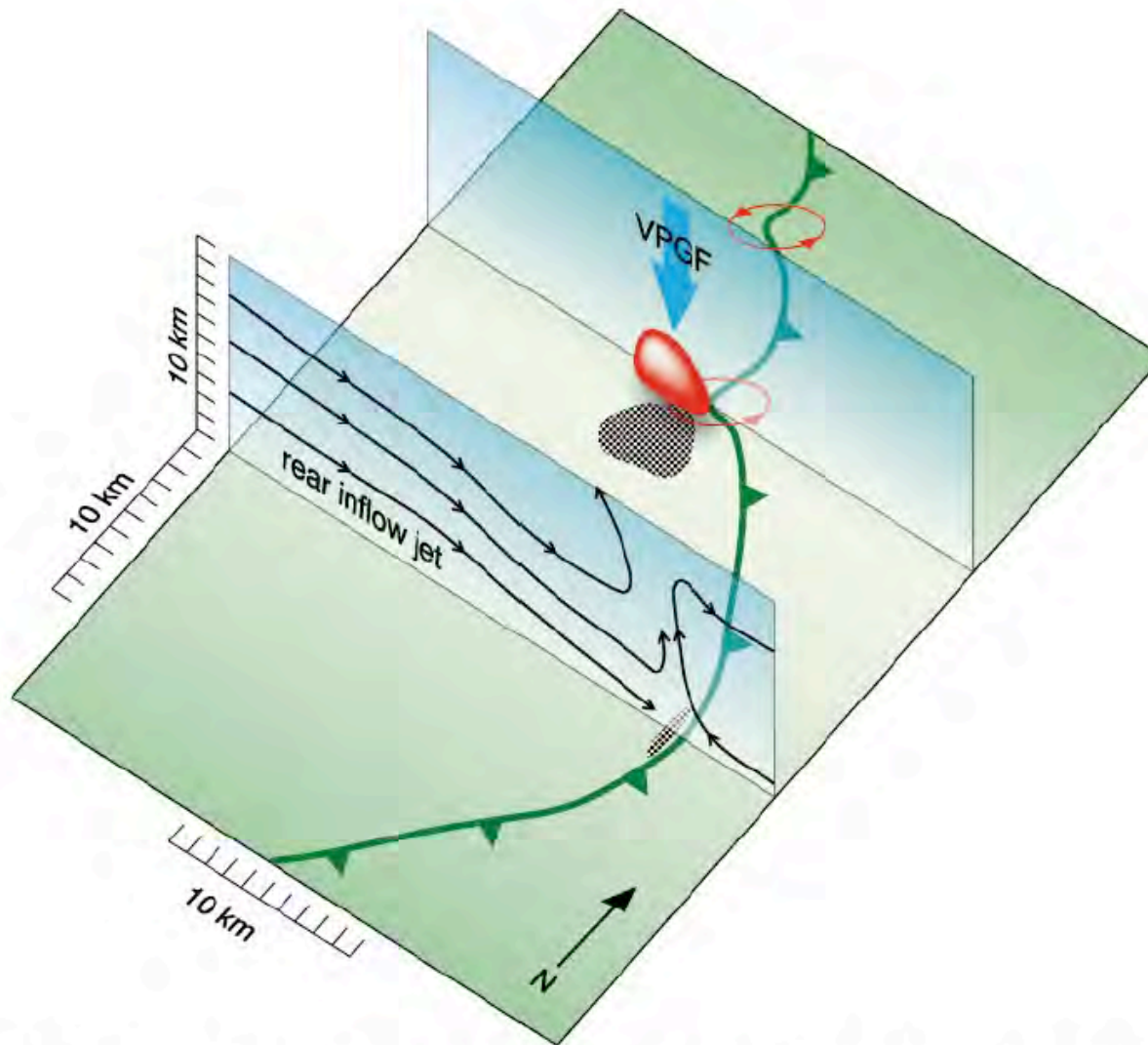


FIG. 24. Schematic showing proposed effect of low-level mesovortices on QLCS structure and also their role in the production of damaging surface winds. The green barbed line indicates gust front and red circles denote low-level mesovortices. The red area in the vertical plane shows vertical extent and tilt of positive vertical vorticity and the corresponding mesovortex. The implication is an associated downward-directed vertical pressure-gradient force (bold blue arrow) that acts to locally eliminate or "fracture" the updraft above the mesovortex location. Black stippling on the south-southwest flank of this mesovortex shows the area of instantaneous damaging "straight line" winds driven by the vortex circulation. A lesser area, or a narrow strip of such winds, is indicated well southeast of the vortex, at the apex of the primary bowing segment. These winds are due to a rear-inflow jet that descends to the ground, represented by the black streamlines in the other vertical plane.



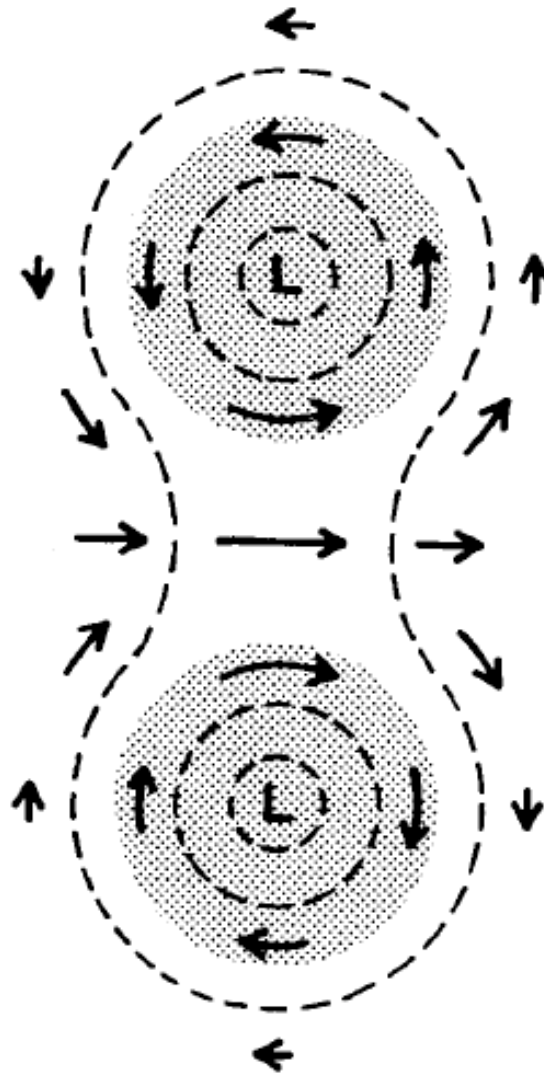


FIG. 21. Schematic representation of an idealized two-dimensional vortex couplet, depicting the stronger flow induced between the vortices. Shading denotes regions of constant vorticity. Unshaded regions have zero vorticity. Dashed contours represent an approximate negative pressure perturbation field that is consistent with the flow pattern. The L denote the locations of the lowest pressure.